Stony Brook University

Phenotypic Characterization of *mIqgap2*-Deficient Mice

A Dissertation Presented

by

Carmine Saverio Chiariello

to

The Graduate School

In Partial Fulfillment of the

Requirements

For the Degree of

Doctor of Philosophy

in

Genetics

Stony Brook University

December 2007

Stony Brook University

The Graduate School

Carmine Saverio Chiariello

We, the dissertation committee for the above candidate for the

Doctor of Philosophy degree,

hereby recommend acceptance of this dissertation.

Wadie Bahou, MD, Dissertation Advisor
Professor of Medicine
Department of Molecular Genetics and Microbiology

James Konopka, PhD, Chairperson of Defense
Professor
Department of Molecular Genetics and Microbiology

Joav Prives, PhD
Professor
Department of Pharmacological Sciences

Nicholas Nassar, PhD
Assistant Professor
Department of Physiology and Biophysics

This dissertation is accepted by the Graduate School

Lawrence Martin
Dean of the Graduate School

Abstract of the Dissertation

Phenotypic Characterization of *mIqgap2*-Deficient Mice

by

Carmine Saverio Chiariello

Doctor of Philosophy

in

Genetics

Stony Brook University

2007

IQ containing GTPase Activating Proteins is a widely conserved family of pseudo-GAPs stretching from *S. cerevisiae* to *H. sapiens*, functioning as multidomain scaffolding proteins capable of integrating cellular signals at cytoskeletal / cell membrane interfaces. Human and murine species express three IQGAPs known to associate with the small GTPases Rac1 and Cdc42, and are regulated by calmodulin in a calcium-dependent manner. Preliminary characterization of *mIqgap2*$^{-/-}$ mice demonstrated age-dependent mortality due to the development of hepatocellular carcinoma. Hepatocellular carcinoma was manifested by loss of membrane bound β-catenin, and upregulation of cyclin D1, suggesting activation of the canonical Wnt/Frizzled pathway. Sera analysis of hepatospecific enzymes and tissue apoptosis staining demonstrated that this phenotype is predated by an age-dependent increase in liver-specific aspartate aminotransferase which correlates to an increase in apoptotic hepatocytes. Furthermore, ultrastructural analysis and functional studies using potentiating dyes in mitochondria suggested an altered metabolic phenotype. In-depth basal metabolic analysis demonstrates that *mIqgap2*$^{-/-}$ mice have higher body fat

composition, decreased basal triglycerides and glucose, and are metabolically more active than wild type. Additionally, *in vitro* and *in vivo* fatty acid experiments showed that *mIqgap2*$^{-/-}$ deficiency results in triglyceride hypersecretion from hepatocytes, and not fatty acid uptake or oxidation. *In vivo* testing using a high fat diet increased *mIqgap2*$^{-/-}$ mouse activity compared to wild type levels. More so, *mIqgap2*$^{-/-}$ mice are protected from steatohepatitis, recapitulating the *in vitro* observation of increased triglyceride secretion, and suggesting fatty acids are a preferred fuel source in these mice. These observations identify IQGAP2 as a novel mediator of hepatic triglyceride partitioning and its effects in metabolic fuel switching, and provide clues to interacting molecular pathways causally linking hepatocellular carcinoma to energy utilization.

Table of Contents

List of Abbreviations

ACBP……...Acyl-CoA Binding Protein
AFB1……..Aflatoxin B-1
ALT……...alanine aminotransferase
AMG4KO…….adipose and muscle specific GLUT4 knockout
AST……...aspartate aminotransferase
BAPTA……1,2-bis(o-aminophenoxy)ethane-N,N,N',N'-tetraacetic acid
CH……..Calponin Homology
CLIP-170…….cyotplasmic linker interacting protein -170
CoA……Coenzyme-A
CPK……Creatine Phosphokinase
CPT…….carnitine palmitoyl transferase
EM…….Electron Microscopy
FA……fatty acid(s)
FABP……..Fatty Acid Binding Protein
FATP……...Fatty Acid Transport Protein
FFA……...free fatty acid(s)
GLUT…….Insulin Responsive Glucose Transporter
GRD……GTPase Regulatory Domain
GTT……glucose tolerance test
GSK-3β…….glycogen synthase kinase-3-beta
H&E……..Hematoxylin & eosin
HB/Cv……..Hepatitis B/C virus
HCC……Hepatocellular Carcinoma
HDL……High Density Lipoprotein
IACUC……...Institutional Animal Care and Use Committee
IDDM…….Insulin-Dependent Diabetes Mellitus
INF-α…….Interferon-alpha
IQ……..Calmodulin Binding Domain
IQGAP……IQ motif containing GTPase Activating Protein
IR…….....Internal Repeat
IR……..……Insulin Receptor
LDL……....Low Density Lipoprotein
MODY……..Mature Onset Diabetes of the Young
NAFLD……..Non-Alcoholic Fatty Liver Disease
NASH……Non-Alcoholic Steatohepatitis
NIDDM…….Non-Insulin-Dependent Diabetes Mellitus
PAR……Protease Activated Receptor
PIP_3…….Phosphotidylinositol-3 phosphate
PI3K……..Phosphotidylinositol-3 phosphate Kinase
PTEN……Phosphotase and Tensin homolog
PTP…….Permeability Transition Pore
RER…….Respiratory Exchange Ratio
ROS…….Reactive Oxygen Species
SREBP-1c……..sterol reactive element binding protein -1c

TG……..triglyceride(s)
TGF-β…….Transforming Growth Factor-beta
TMRE…….tetramethyl rhodamine ethyl ester
TNF-α.....Tumor Necrosis Factor-alpha
TUNEL……TdT-mediated biotin 16-dUTP nick-end labeling
WW…….Tryptophan-rich Domain
vLDL……..very low density lipoprotein

List of Figures

List of Tables

Acknowledgements

Throughout my tenure in graduate school, I have learned much, both scientifically and in life, and moreso how one greatly affects the other. I would like to express my sincerest thanks to Dr. Wadie Bahou for his mentorship and understanding throughout many milestones in my life during these past years. Also, I wish to thank my graduate committee for their help and advice.

To Jun Xu, without whom, parts of this dissertation were not possible. His assistance in the calorimetry experiments and interpretation of data is invaluable. I thank him for allowing me to utilize the insulin and glucose tolerance test data in this dissertation.

To my family, whose support, encouragement, and life lessons are invaluable to any child and brother.

To my wife Colleen and my little angel Maria Grace, my true passions in life, thank you for the one thing that matters most, being there.

Figures in this Dissertation were Reprinted by Permission from Macmillan Publishers Ltd: Nature Reviews Cancer, **Farazi PA and DePhino RA.** Hepatocellular carcinoma pathogenesis: from genes to environment. *Nat Rev Cancer* 6:674-687, 2006 © 2006.

Springer and Mammalian Genome, vol 15, 2004, p618-629, Distinct PAR/IQGAP expression patterns during murine development: implications for thrombin-associated cytoskeletal reorganization, Cupit LD, Schmidt VA, Miller F, Bahou

I. Age-Dependent Hepatopathy in *mIqgap2*$^{-/-}$ Mice

Background

IQ containing GTPase Activating Proteins (IQGAPs)

IQGAP2 is a member of a widely conserved eukaryotic family of homologous GTPase Activating Proteins. IQGAP homologs have been identified in a broad range of species, from yeast (*S. cerevisiae,* Iqg1p/Cyk1p)(42, 84, 98) to hydra (*H.vulgaris*, IQGAP1)(124) to man (*H. sapiens,* IQGAP1)(130) (**Figure 1**). The yeast proteins Iqg1p/Cyk1p and Rng2p contain sequence structure similar to *H. sapiens* IQGAP1 (hsIQGAP1), and participate in similar function(89). However, homologs from amoeba (*D. discoideum*, GAPA, DGAP1) display sequence similarity to the C-terminus of hsIQGAP1(89). More so, the similarity of GAPA and DGAP1 allow for functional redundancy in amoeba. The single DGAP1^{-} mutant has no cytokinetic impairment, the double knockout DGAP1^{-}/GAPA^{-} is defective in cytokinesis(44). To date, in human and mouse, three IQGAP paralogs have been identified (IQGAP1, -2, and -3)(91, 127, 130), where IQGAP1 has been best characterized biochemically. Initial reports identified a broad tissue expression patterning of IQGAP1(130) while IQGAP2(91) retained liver-specific expression. Recent work has expanded the mRNA expression patterning of IQGAP2 to concomitant tissues with IQGAP1 (**Figure 2A**), although no protein evidence exists to support this observation (29). Furthermore, IQGAP2 is syntenically expressed within the Protease Activated Receptor (PAR) gene cluster on mouse chromosome 13 and human chromosome 5 (**Figure 2B**),

Figure 1

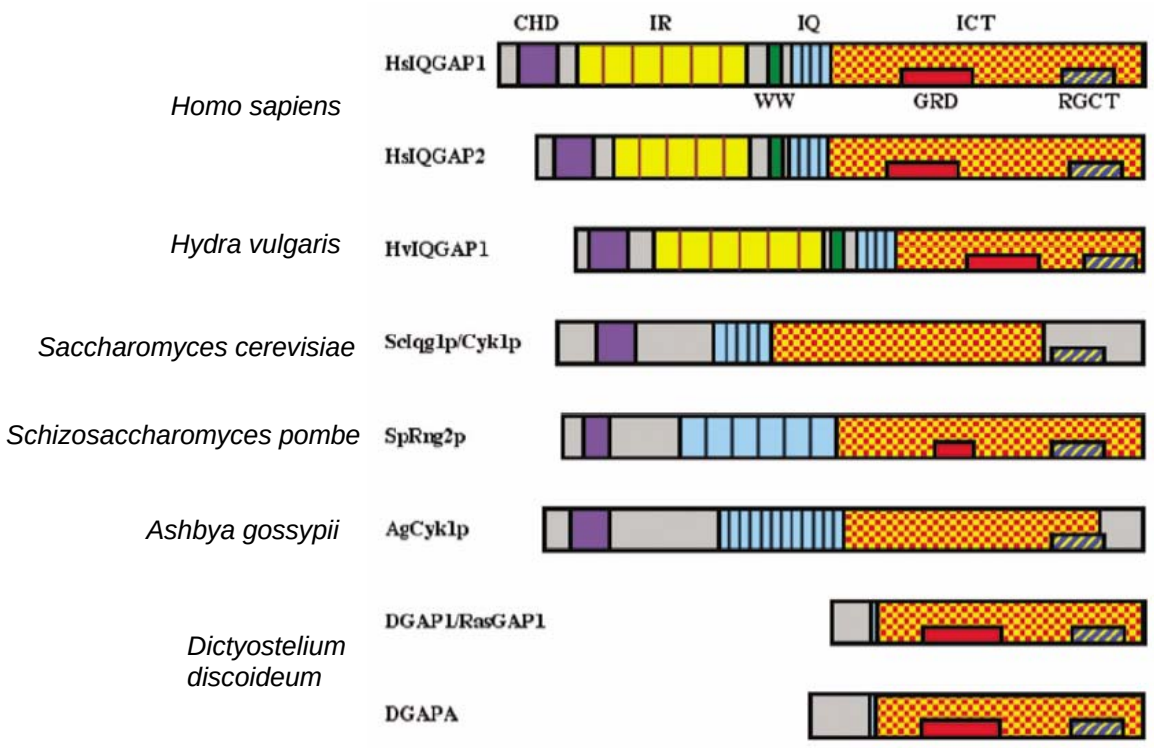

Mateer, et al 2003

Domain Key:

CH = Calponin Homology
IR = Internal Repeat
WW = Tryptophan (W) rich motif
IQ = Isoleucine – Glutamine rich motif
GRD = GTPase Regulatory Domain
ICT = IQGAP C-terminal region
RGCT = RasGAP-like C-terminal region

Figure 1: IQGAPs are diversely expressed scaffolding proteins. IQGAP proteins are conserved from *D. discoideum* to *H. sapiens* and share similar C-terminal structure. Domain abbreviations: CH: Calponin Homology; IR: Internal Repeat; WW: Tryptophan-rich motif; IQ: Isoleucine-Glutamine-rich motif; GRD: GTPase Regulatory Domain; ICT: IQGAP C-terminal region; RGCT: RasGAP C-terminal region.

Figure 2

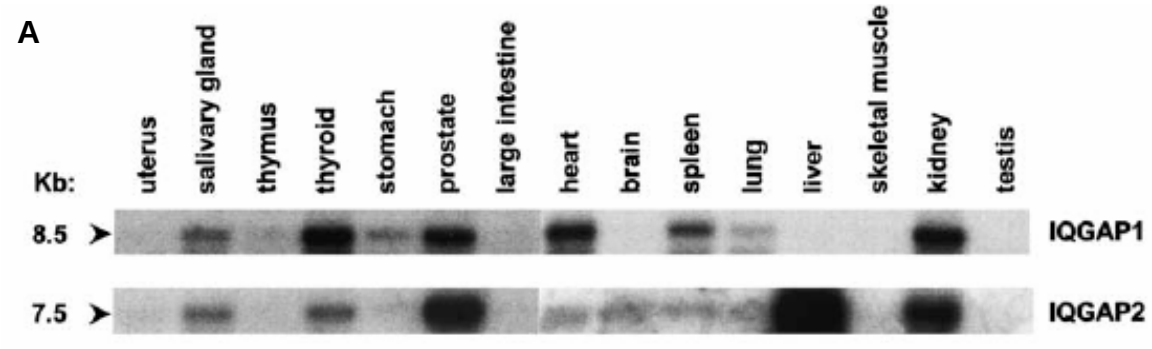

Cupit, et al 2004

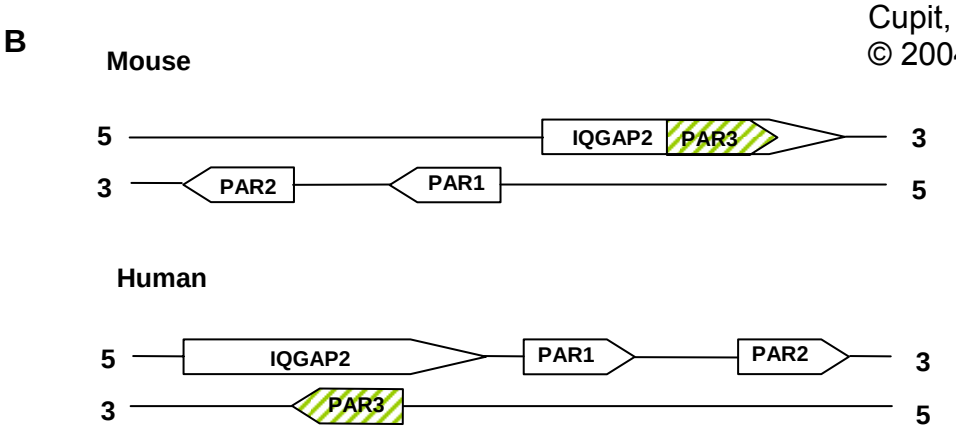

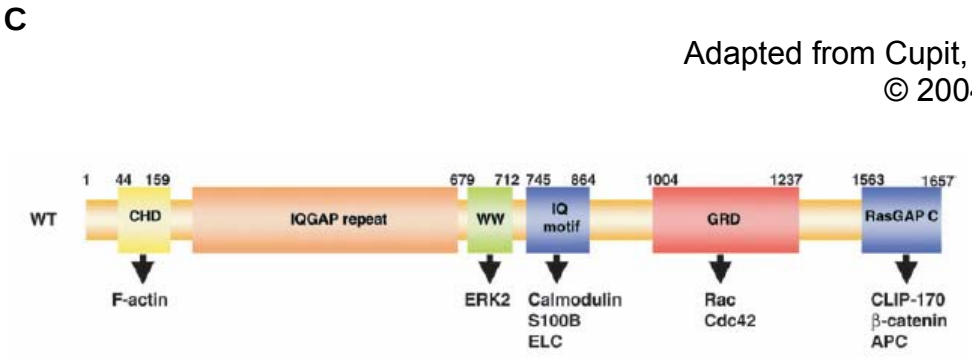

Adapted from Cupit, et al 2004

Noritake, et al 2005

Figure 2: IQGAPs are multidomain scaffolding proteins expressed in various tissues. (**A**) mRNA expression patterning of *mIqgap1* and *mIqgap2* in murine tissues reveals broad expression patterning. (**B**) *In silico* genomic analysis demonstrates that *IQGAP2* is syntenically located on murine and human chromosome 13 and 5, respectively. More so, *Iqgap2* genes are located within the PAR gene cluster, suggesting the possibility of hematopoietic gene regulation. (**C**) Sequence identification of *hIQGAP1* reveals the multidomain organization of IQGAP1 which is capable of binding the GTPases Rac1 and Cdc42 at the actin cytoskeleton. IQGAPs are also modulated by calcium signaling via calmodulin interaction.

implicating the possibility of hematopoietic regulation and platelet-specific expression(29, 113).

Biochemical Characterization of IQGAPs

IQGAPs are multidomain scaffolding proteins that allow integration of multiple cellular events at the cell membrane (**Figure 2C**) Human (hsIQGAP) and murine (mIQGAP) proteins contain an N-terminal Calponin Homology (CH) domain, capable of binding actin(88), 5 internal repeat (IR) domains implicated in homo- and heterodimerization(109), tryptophan (WW) rich domain capable of binding proline rich motifs(87), 4 Ca^{+2}-modulated domains (IQ), with the conserved motif IQXXXRGXXR, known to bind calmodulin(82, 130), and a GTPase regulatory domain (GRD) known to bind Rac1 and Cdc42(64, 76). GTPase binding to IQGAPs preferentially occurs in the active, GTP-bound state. The GRD domains of IQGAP proteins lack a critical arginine finger required for the function of promoting GTP hydrolysis by GTPases(89). This dominant activating function of IQGAPs allows bound GTPases to be sequestered in an active state, promoting the formation of filipodia, as in the case of Cdc42(76). More so, elimination of the IQGAP1 GRD domain decreases the available pool of active Cdc42 and results in subcellular mislocalization(119). These experiments detailed IQGAP1 as necessary for Cdc42 function at cell membrane locales. Furthermore, IQGAP1 recruitment of active Rac1 is required for cell surface maintenance of E-Cadherin(64). E-Cadherin based cell-cell adhesion is tightly associated with β-catenin. Loss of either active Rac1 or IQGAP1 destabilizes the cadherin-catenin complex through competitive binding of IQGAP1 to β-catenin,

indicating that active Rac1 is required for IQGAP1 - β-catenin dissociation, and therefore E-Cadherin cell surface stabilization(64). Recently, IQGAP1 was shown to bind cytoplasmic linker interacting protein (CLIP-170), a microtubule plus-end binding protein(54). This suggests IQGAP1 binding to CLIP-170 serves as a convergence point for Rac1 and Cdc42-related signaling at the actin and microtube cytoskeletal networks in a calcium-dependent manner(58).

Modulation of IQGAPs by calcium/calmodulin

Calcium is a major chemical messenger capable of modulating multiple cellular events(61, 89, 90), in which calmodulin serves as the mediator. Work detailing the role of calcium regulation of IQGAPs suggest they are negatively regulated by calmodulin in a calcium-dependent manner(61, 67, 80). Experiments eliminating endogenous calmodulin revealed that a vast majority of cellular calmodulin is bound to IQGAP1 in a calcium-dependent manner(61). More so, apocalmodulin is constitutively bound to IQGAP1 on the 3rd and 4th IQ repeats where calcium/calmodulin binds all 4 IQ motifs(67). This would suggest that the binding of calcium to calmodulin induces a transient conformational change in IQGAPs, reducing their ability to modulate GTPase function. Indeed, addition of calcium *in vitro* eliminated the interaction between IQGAP1 and Cdc42, which also inhibited the formation of F-actin(53). Another regulation of IQGAPs by calmodulin is by altering subcellular localization. Calmodulin is known to bind and alter localization of p21(121) and Rad(95) in a calcium-dependent manner. Recent work revealed that binding of calcium/calmodulin displaces

IQGAP1 from the cell membrane to the cytosol(82), thereby negatively regulating its function.

Physiological Characteristics of IQGAP knockouts

While IQGAP1 has been demonstrated to bind actin and modulate cadherin-based adhesion through competitive inhibition of catenin/cadherin complex formation with regulation by GTPases Rac1 and Cdc42 as well as calcium/calmodulin, the physiological significance of these biochemical interactions has not been fully investigated. Observations of *mIqgap1* knockout mice demonstrate the age dependent development of gastric hyperplasia(81), with minimal explorations as to the molecular mechanism underlying this pathology. A possible explanation for the mild phenotype is the functional redundancy between the other paralogs, IQGAP2 and IQGAP3. Work from our lab has further expanded the *mIqgap1*$^{-/-}$ phenotype by elucidating the role of IQGAP1 in shear-restricted activation of platelets (4).

Recently, our lab has generated a *mIqgap2* knockout mouse which succumbs due to hepatocellular carcinoma (HCC)(112). Furthermore, this pathology is due to the negative regulation of IQGAP1 and activation of β-catenin, allowing nuclear translocation and upregulation of cell cycle genes, in particular, cyclin D1(112)(**Figure 3**).

Epidemiology and Etiology of Hepatocellular Carcinoma

Causative Factors and Progression of Hepatocellular Carcinoma

HCC is the major contributor to all reported human liver cancers(38). While infrequent in the United States, the majority of reported

Figure 3

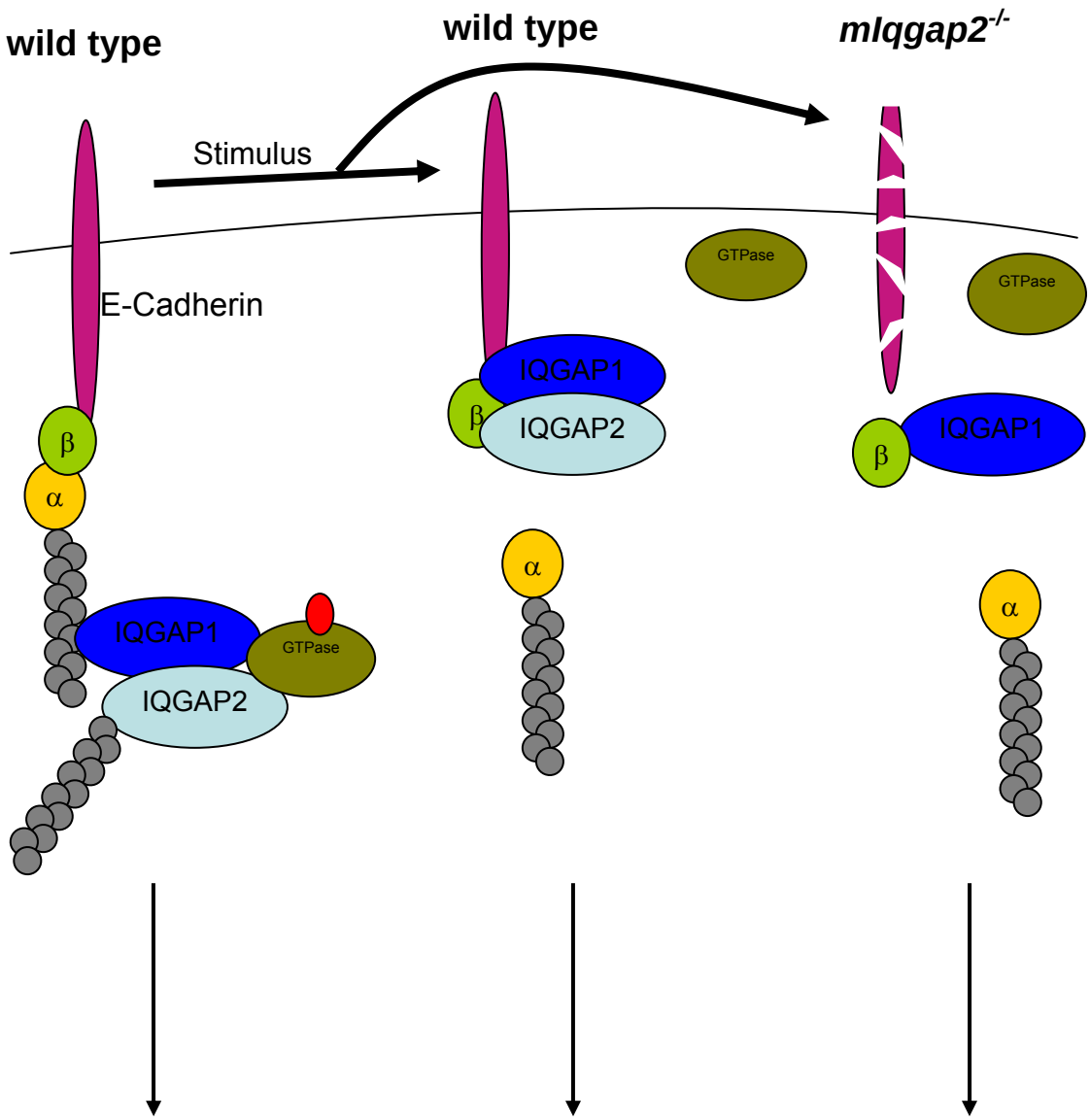

- Cell stability
- Strong cadherin based adhesion

- Cell motility / weak adhesion
- Cell membrane β-catenin stabilization

- IQGAP1 instability / β-catenin translocation
- E-Cadherin degradation

Adapted from Noritake, et al, 2005

Figure 3: Model for IQGAP2-based cadherin/catenin/IQGAP1 stability and the role in hepatocarcinogenesis. During cell quiescence, IQGAPs are bound to active GTPases and allow for actin crosslinking/stability. However, after stimulation and GTPase hydrolysis of GTP, IQGAPs dissociate from GTPases and competitively bind β-catenin (β) by displacing α-catenin (α). Furthermore, IQGAP2 binding of IQGAP1 allows for catenin/cadherin stability. However, in *mIqgap2*$^{-/-}$ mice, loss of IQGAP2-mediated stability of cadherin/catenin/IQGAP1 complexes results in degradation of E-cadherin and loss of membrane-localized β-catenin, resulting in nuclear translocation of β-catenin and activation of the cell cycle gene, cyclin D1. The retained association between IQGAP1 and β-catenin allows for β-catenin stability and protection from proteasome degradation. This may serve as the genetic modality by which HCC develops in *mIqgap2*$^{-/-}$ mice.

Image adapted from Noritake, et al, 2005, © The Company of Biologists

cases are located in Asia and sub-Saharan Africa(131). Numerous epigenetic factors contribute to the onset of HCC, such as chronic hepatitis infection, fungal toxin infection, alcoholism, and chronic fatty dieting(38, 45). However, chronic viral hepatitis B and C (HB/Cv) infections are the major causative factors.

The progression of the disease state is a phasic process. Causative factors (infection, heredity, alcohol, etc) damage hepatic tissue through multiple mechanisms such as increased reactive oxygen species (ROS) exposure, inflammation, and genomic instability (**Figure 4A**). The hepatic response is manifested as localized necrosis / apoptosis which surrounding healthy tissues compensate by increased proliferation. Chronic injury perpetuates numerous cycles of necrosis and proliferation resulting in localized fibrosis, characterized by nodules of collagenic scar tissue. These fibrous nodules further develop cirrhosis. Associated genomic instability progresses in these hyperplastic nodules, eventually leading to cancer (**Figure 4B**)(45).

Hepatitis Infection

Chronic HB/Cv exposure is the major contributing factor to HCC development(77). The ability of certain HB/Cv proteins to interact with mediators of the cellular immune response, such as tumor necrosis factor-α (TNF-α) and interferon-α (IFN-α), and evade immune-related signaling create an advantageous replicative environment(93, 101). However, the integration of viral DNA is not a requirement for replication, suggesting the relationship between HCC and HB/Cv infection is causal. Furthermore, chronic exposure increases the frequency of viral DNA propagation into host genomes, either deleting host

Figure 4

A

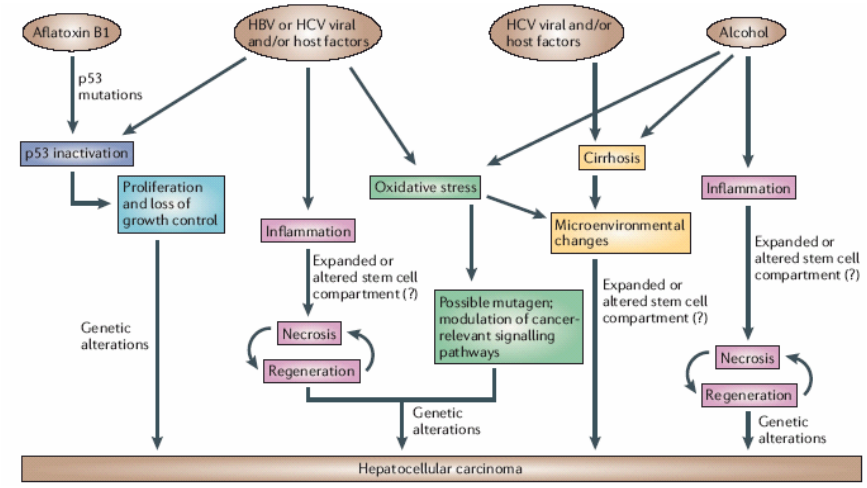

Farazi, PA, DePhino, 2006
© Nature Publishing Group

B

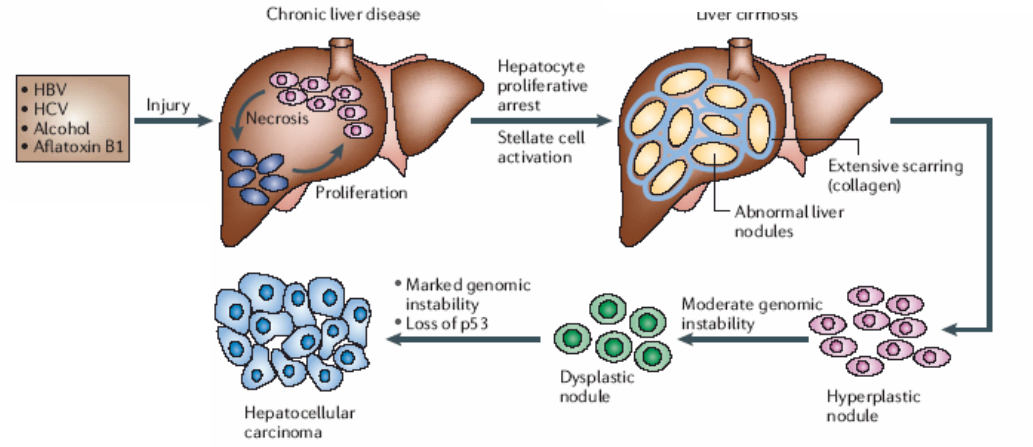

Farazi, PA, DePhino, 2006
© Nature Publishing Group

Figure 4: Etiology and progression of hepatocellular carcinoma. (A) Multiple risk factors of HCC participate in various mechanisms which progress the disease state. **(B)** Following injury, hepatocytes undergo localized necrosis, which is initially complemented by hepatic proliferation. This necrotic-proliferative cycle results in cirrhotic nodules, followed by hyperplastic, then dysplastic nodules. Loss of genomic stability either through genetic mutations or telomerase activation are culminating factors in hepatocarcinogenesis.

genomic DNA resulting in loss of heterozygosity(110), or disrupting coding sequence through insertional mutagenesis(102).

Chemical Hepatocarcinogens

The *Aspergillus* mycotoxin aflatoxin is a potent carcinogen common to humans and livestock, mainly though contamination of food products(45). Eighteen isoforms of aflatoxin exist, with B1, B2, G1, and G2 being the predominant compounds found in nature(79). Aflatoxin B1 (AFB1), the most potent aflatoxin, is correlated with incidences of HCC(38, 79). Studies to understand the molecular action of AFB1 using stable chemical analogs revealed AFB1 binds host genomic DNA resulting in base pair mutations(92, 126). Genomic hotspots correlated with hepatic function and cell cycle regulation have been identified in AFB1 induced HCC. High incidences of A249S missense mutations in p53 have been identified in HCC cases reported in China and Africa(16). This alteration in *TP53* is disproportionately higher than non-mycotoxin related carcinomas, and may serve as a clinical marker for aflatoxin induced HCC.

Vinyl chloride is a major hepatocarcinogen found in industrial settings(71), and exposure is often through direct inhalation of vinyl chloride gas or inhalation of polyvinyl chloride particulates. Hepatotoxicity results from mitochondrial metabolism of vinyl chloride into the more labile compound chloroethylene oxide, which has the capacity to covalently modify nucleotides(71). Interestingly, mutagenic hot spots in both *TP53* as well as *ras*

genes have been identified in vinyl chloride-induced genotoxicity, many involving A-T base pair substitutions(7, 32).

Alcoholism and Obesity

Chronic alcohol exposure also plays a role in the onset and progression of HCC. However, the heterogeneous effects of alcohol on the body make it difficult to elucidate its role in the progression of HCC. One possible means by which excessive alcohol intake increases the incidence of HCC is through the formation of ROS. Accumulation of ROS results in intrahepatic damage, lipid peroxidation and hepatic apoptosis. Chronic alcohol exposure progresses localized cell death to fibrosis, and then cirrhosis, a major precursory event to HCC. While incidences of alcohol-induced HCC are quite low(38), synergistic effects occur when consumption of alcohol is coupled with HB/Cv infection or hereditary predisposition.

Excessive dietary fat intake is the least known causative factor in the development of HCC. Yet, like alcohol, the effects of excessive fat intake in the development of nonalcoholic fatty liver disease (NAFLD) or nonalcoholic steatohepatitis (NASH) have synergistic effects when coupled to other epigenetic factors such as HB/Cv infection. Studies in groups diagnosed with NAFLD or groups that were followed after diagnosis developed HCC in only 0.5% of the population, whereas predictable outcomes of obesity and diabetes were more prevalent(3).

Genetics of Hepatocellular Carcinoma

Numerous hereditary genetic aberrations have also been attributed to the onset of HCC. While the complexities of human studies have generated a milieu of genetic precursors for HCC, genes involved in relevant physiological pathways have been identified to be mutated in hepatocarcinogenesis.

Aberrations of the PI3 Kinase (PI3K) / Akt pathway is reported in 40-60% of HCC cases(63). Aberrations in expression of phosphatase and tensin homolog gene (*PTEN*), the phosphatase responsible for negative regulation of PI3K via dephosphorylation of phosphatidylinositol 3,4,5- phosphate (PIP_3), account for the majority of PI3K / Akt derived HCC(62), and could account for the suppression of transforming growth factor-β (TGF-β) induced hepatocyte apoptosis(38). The loss of PTEN function would allow for PI3K activation and progression into the cell cycle and eventual malignant transformation.

Nearly 1/3 of human HCC is derived from mutations in β-catenin (*CTNNB1*), a downstream effector of the Wnt / Frizzled cascade(31). β-catenin is an adapter protein, linking cadherins to the cytoskeleton. Under basal conditions, β-catenin is coupled to E-Cadherin at the cell membrane, along with α-actinin, Rac1, Cdc42, IQGAP1, and IQGAP2. The dissociation of β-catenin from cell membrane locales allows for nuclear translocation and upregulation of the cell cycle regulator cyclin D1(17, 112). Deletion of liver-specific adenomatosis polyposis coli (*Apc*), a protein involved in β-catenin degradation, allows for activation of β-catenin with subsequent formation of HCC(26).

As previously stated, our lab had created a *mIqgap2*-deficient mouse which develops age-dependent HCC(112). In hepatocytes, IQGAP2 acts as a tumor suppressor, prohibiting activation of the Wnt / β-catenin pathway via negative regulation of IQGAP1(112). Coimmunoprecipitation experiments demonstrated that IQGAP2 binds β-catenin and IQGAP1, but not E-Cadherin, whereas IQGAP1 binds IQGAP2, β-catenin, and E-Cadherin(112). Analysis of tumor tissue from HCC-positive *mIqgap2*$^{-/-}$ mice showed deregulation of the cadherin-catenin complex characterized by loss of cell surface expression of E-Cadherin and nuclear translocation of β-catenin, followed by upregulation of the cell cycle gene cyclin D1(112). Furthermore, Kaplan-Meier analysis of wild type, *mIqgap2*$^{-/-}$, and *mIqgap1*$^{-/-}$/*mIqgap2*$^{-/-}$ mice reveals progressive mortality of *mIqgap2*$^{-/-}$ mice versus wild type and *mIqgap1*$^{-/-}$/*mIqgap2*$^{-/-}$ mice, beginning at approximately 6 months(112). The indistinguishable mortality rates between wild type and *mIqgap1*$^{-/-}$/*mIqgap2*$^{-/-}$ mice, in conjunction with the observation that *mIqgap1*$^{-/-}$/*mIqgap2*$^{-/-}$ mice do not succumb to HCC reinforce the idea that IQGAP2 is a potential negative regulator of IQGAP1 (**Figure 3**)(112).

Here we describe the preneoplastic state of *mIqgap2*$^{-/-}$ hepatocytes, characterized by an age-dependent increase in apoptotic hepatocytes, paralleled with increasing serum aspartate aminotransferase (AST) but not alanine aminotransferase (ALT), defective mitochondrial morphology, and inability for *ex vivo* viability.

Materials and Methods

Histochemistry and Electron Microscopy

Generation of IQGAP2-deficient mice on the 129J1 background was described previously(112). All animal studies were performed following strict guidelines as approved by the Stony Brook Institutional Animal Care and Use Committee (IACUC) as well as criteria outlined in the NIH *Guide for the Care and Use of Laboratory Animals*. For histochemistry, wild type or *mIqgap2*$^{-/-}$ mice, 1, 4, 8 and 12 months of age were sacrificed under Metofane anesthesia (Methoxyflurane USP, Medical Developments International Ltd., Melbourne, Australia) and livers immediately fixed in 10% neutral buffered formalin overnight at 4^{O}C. Paraffin embedding, sectioning and Hematoxylin & Eosin (H&E) staining of liver sections was performed at Stony Brook University Hospital Histology Laboratory and sections analyzed for gross morphology.

For electron microscopy, isolated livers were immediately submerged in EM fixative (5% gluteraldehyde, 4% formaldehyde in 0.008 M Phosphate Buffer, Electron Microscopy Sciences, Fort Washington, PA) overnight at 4^{O}C. Mounting, sectioning, and analysis performed at Stony Brook University Microscopy Imaging Center.

Biochemical Analysis

Overnight fasted mice at 1, 4 or 8 months of age were bled under Metofane anesthesia by retro-orbital puncture. 200 μl of whole blood was collected and allowed to clot at room temperature for 1 hour. Coagulated blood

was spun at 14,000 x g for 5 minutes and serum removed. Levels of aspartate aminotransferase (AST), alanine aminotransferase (ALT), cholesterol, total and direct bilirubin, high density lipoproteins (HDL), and creatine phosphokinase (CPK) were obtained using a MODULAR PP serum work area analyzer at Stony Brook University Hospital (Roche Diagnostics, Indianapolis, IN)(4).

Hepatocyte TUNEL Assay

The quantification of apoptotic hepatocytes was accomplished using TUNEL staining. Briefly, 1, 4 and 8 month wild type and *mIqgap2*$^{-/-}$ mice were sacrificed under Metofane anesthesia and livers isolated. After overnight fixation in 10% neutral-buffered formalin, livers were sent to Stony Brook University Hospital Histology Laboratory for mounting and sectioning (5 μm thick). Sections were then deparaffinized in xylene and rehydrated in decreasing concentrations of ethanol (100 – 0 %) for 5 minutes each. Sections were then digested with 20 mg/ml proteinase K for 10 minutes at room temperature, washed and quenched in 3% hydrogen peroxide in PBS for 10 minutes at room temperature. Quenched sections were then incubated with TdT enzyme for 60 minutes at 37^{O}C for end labeling with dUTP (Chemicon). Following labeling, sections were incubated with a digoxigenin-conjugated anti-dUTP antibody for 60 minutes at room temperature. Hybridized sections were then washed and detected using DAB substrate until sufficient coloring was observed. Labeled sections were then counterstained with methyl green and mounted in Permount. Apoptotic cells

were scored and quantified (1,000 cells per section) by 2 independent investigators.

Mitochondrial Assays

Mitochondria were isolated from livers isolated from 1, 4 and 8 month wild type and *mIqgap2*$^{-/-}$ mice that were sacrificed under Metofane anesthesia. Livers were subjected to isotonic homogenization in ice-cold lysis buffer (0.25 M sucrose, 10 mM HEPES, pH 7.4, 1 mM EGTA). The mitochondrial fraction was isolated by differential centrifugation at 4^{O}C. Isolated mitochondria were resuspended in isolation buffer (210 mM mannitol, 70 mM sucrose, 20 mM HEPES, pH 8.0, 2 mM EDTA, 2 mM DTT and protease inhibitors)(13). A 100 μl aliquot of mitochondria was used for BCA protein quantification (Pierce, Rockford, IL). For functional studies, 100 mg of mitochondrial protein was loaded with 50 mM tetramethyl rhodamine ethyl ester (TMRE) for 10 minutes at room temperature. To assay for sensitivity of the permeability transition pore (PTP), mitochondria were incubated with varying doses of valinomycin (0.1, 1, 10, 100 nM) or calcium (0.1, 1, 10, 100 μM) at the same time as TMRE loading. Analysis was performed by FACScan using logarithmic gain settings for fluorescence and light scatter (Becton-Dickenson, Mountain View, CA). For all studies, 10,000 gated events were counted.

Adhesion / Viability Assays

Hepatocytes were isolated from wild type and *mIqgap2*$^{-/-}$ livers by modified collagenase perfusion(73). Briefly, Metofane-anesthetized mice were perfused through the portal vein with 25 ml warmed Perfusion Buffer (Invitrogen, Carlsbad, CA) followed by 25 ml Digestion Buffer (Invitrogen), both at a flow rate of 4ml/min. After perfusion, livers were immediately excised, submerged in 40 ml ice-cold Wash Buffer (Invitrogen) and gently ruptured to disperse hepatocytes. Cells were spun at 50 x g for 5 minutes at 4^{O}C, and the crude pellet was then resuspended in ice-cold Wash Buffer and passed through 3 layers of sterile gauze. The isolated hepatocytes were pelleted and washed 3 more times using Wash Buffer and then resuspended in 2 ml antibiotic-free DMEM without serum. Viability was determined using Trypan Blue exclusion. Hepatocyte preparations exhibiting 80 – 85% viability were used. Isolated hepatocytes were plated at a density of 5x10^{3} cells/well in triplicate on various cell matrices (collagen I, laminin, fibronectin, fibrinogen, BSA, and no coating). Cells were allowed to adhere overnight at 37^{O}C. Viability assays were performed according to CellTiter 96 Proliferation assay (Promega, Madison, WI). Briefly, 15 μl of dye solution was added to wells and incubated for 1 hour at 37^{O}C. 200 μl solubilization solution was then added and allowed to stand 1 hour at RT. Plates were mixed and read at 570nm to quantify viable hepatocytes.

Immunofluorescence of Liver Sections

Modified immunofluorescence(113) analysis was performed on 8 μm thick fresh frozen liver sections obtained from 1, 4, and 8 month old wild type and *mIqgap2*$^{-/-}$ mice. Mice were sacrificed under Metofane anesthesia and livers immediately removed and submerged in cryosectioning medium (OCT compound, Sakura FineTek, Japan). Sections were washed 3 times with PBS to remove mounting medium followed by fixation with 10% neutral buffered formalin. Fixed sections were washed and permeabilized with a 2:1 solution of ethanol : acetic acid for 5 minutes at -20^{O}C. After washing, slides are blocked with Blocking solution (5% normal goat serum, 1% BSA, 0.1% Triton-X 100 and 0.05% Tween-20 in PBS) for 1 hour at room temperature followed by incubation for 1 hour at room temperature with primary antibody diluted in Blocking solution. Hybridized sections are washed with PBS and incubated in appropriate secondary antibody diluted in Blocking solution for 1 hour at room temperature. After washing, sections were mounted in AntiFade Gold (Molecular Probes, Eugene, OR) and visualized using confocal microscopy (Leica Microsystems, Wetzlar, Germany). Primary antibodies used include IQGAP2 (1:1000, Upstate), actin (1:500 TRITC-phalloidin, Molecular Probes), calmodulin (1:1000, Zymed), and E-Cadherin (1:1000, BD Biosciences).

Immunoblotting of Liver Homogenates

Immunoblotting(4) was performed on liver lysates from wild type, heterozygous and *mIqgap2*$^{-/-}$ mice. Mice 1, 4, and 8 months of age were

sacrificed under Metofane anesthesia, livers immediately excised, washed of excess blood, and homogenized in RIPA lysis buffer (50mM Tris, pH 7.4, 150 mM NaCl, 1 mM EDTA, 1% Triton-X 100, 1% Na-deoxycholate, 0.1% SDS, 1 mM phenylmethylsulfonyl fluoride (PMSF), 5μg/ml leupeptin / aprotinin mix) using a Dounce homogenizer (25 strokes). After 20 minute incubation on ice, lysates were spun at 14,000 x g to remove insoluble material. Protein quantification was performed on lysate supernatants using BCA methodologies (Pierce, Rockford, IL). 10 μg of total protein was electrophoretically fractionated using SDS-PAGE, transferred to nitrocellulose, and probed for IQGAP1 (1:1000, Upstate/Millipore), IQGAP2 (1:1000, Upstate/Millipore), E-Cadherin (1:500, BD Biosciences), Calmodulin (1:1000, Zymed), Rac-1 (1:500, BD Biosciences), Cdc42 (1:1000, BD Biosciences), actin (1:500, Chemicon), and GAPDH (1:2000, Chemicon). Detection was accomplished using the appropriate HRP-labeled secondary antibody and enhanced luminescence (Pierce).

Statistical analysis

Results are expressed as the mean ± SEM of appropriate replicates and normalized to protein concentration where necessary. P values are calculated using unpaired Student's t-test, with $p<0.05$ considered statistically significant.

Results

Loss of IQGAP2 does not alter expression levels of known binding partners.

Preliminary observations of *mIqgap2*$^{-/-}$ mice reveal they are healthy, fertile and physically indistinguishable from wild type. Based on murine tissue IQGAP2-expression patterning(19, 29), we predicted there to be a hepatocyte restricted pathology, in particular a loss in either IQGAP2-associated protein stability or cell localization. Analysis of liver lysates reveals no alteration in expression levels of IQGAP-associating binding partners at either 1, 4 or 8 months of age (**Figure 5A,** 1 and 8 months not shown). More so, immunofluorescent analysis of liver sections reveals predictable loss of IQGAP2 staining from cell membrane areas, yet no subcellular differences in actin, E-cadherin, or calmodulin (**Figure 5B**, 1 and 8 months not shown).

Age-dependent increase in the number of apoptotic hepatocytes is observed in *mIqgap2*$^{-/-}$ mice.

To delineate any potential hepatopathy in *mIqgap2*$^{-/-}$ mice, hematoxylin and eosin (H&E) staining of liver tissues was performed. As shown in **Figure 6**, 8 month *mIqgap2*$^{-/-}$ liver sections display an abnormal cellular gradient, extending from the portal triad to the central vein. The gradient is defined by the observed morphology of hepatic nuclei. In wild type, smaller nuclei are observed to penetrate about 30% towards the central vein, whereas larger nuclei occupy the remaining 60% of the lobule. More so, the 2 populations of nuclei are relatively

Figure 5

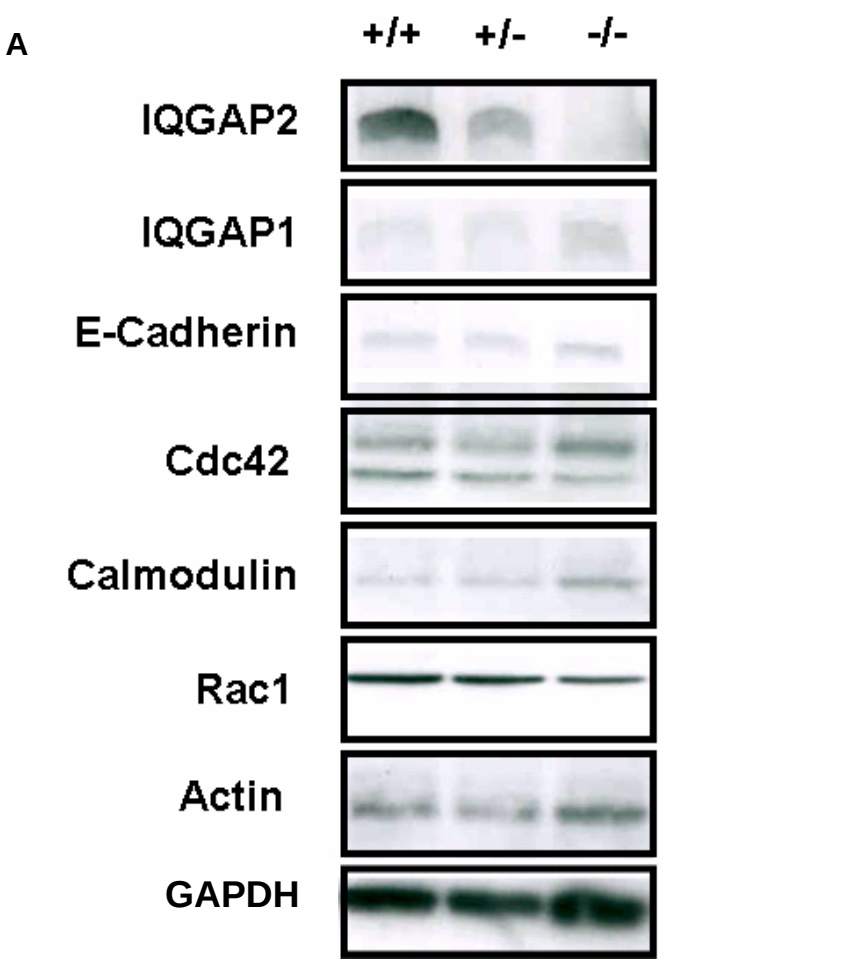
A
+/+
+/-
-/-
IQGAP2
IQGAP1
E-Cadherin
Cdc42
Calmodulin
Rac1
Actin
GAPDH
B
IQGAP2
actin
calmodulin
E-Cadherin
wild type
mIqgap2-/-

Figure 5: Neither expression patterning nor subcellular localization of certain IQGAP2 binding proteins is affected in *mIqgap2*$^{-/-}$ hepatocytes. (**A**) Livers from 4 month old wild type, *mIqgap2*$^{+/-}$ and *mIqgap2*$^{-/-}$ mice were homogenized and 15 μg of total protein fractionated using SDS-PAGE and probed for IQGAP2-associating proteins. Antibodies used were directed against actin, IQGAP1, E-Cadherin, Cdc42, calmodulin, and Rac1. GAPDH was used as a loading control. (**B**) Livers from 4 month wild type and *mIqgap2*$^{-/-}$ mice were removed, immediately submerged in cryosectioning medium and frozen at -80^{O}C overnight. Livers were sectioned at 8μm. After washing, sections were blocked for 1 hour at room temperature and then probed with antibodies against IQGAP2, actin, calmodulin, or E-Cadherin. AlexaFluor-488 conjugated secondary antibodies were incubated for one hour followed by washing and mounting in Antifade Gold solution.

Figure 6

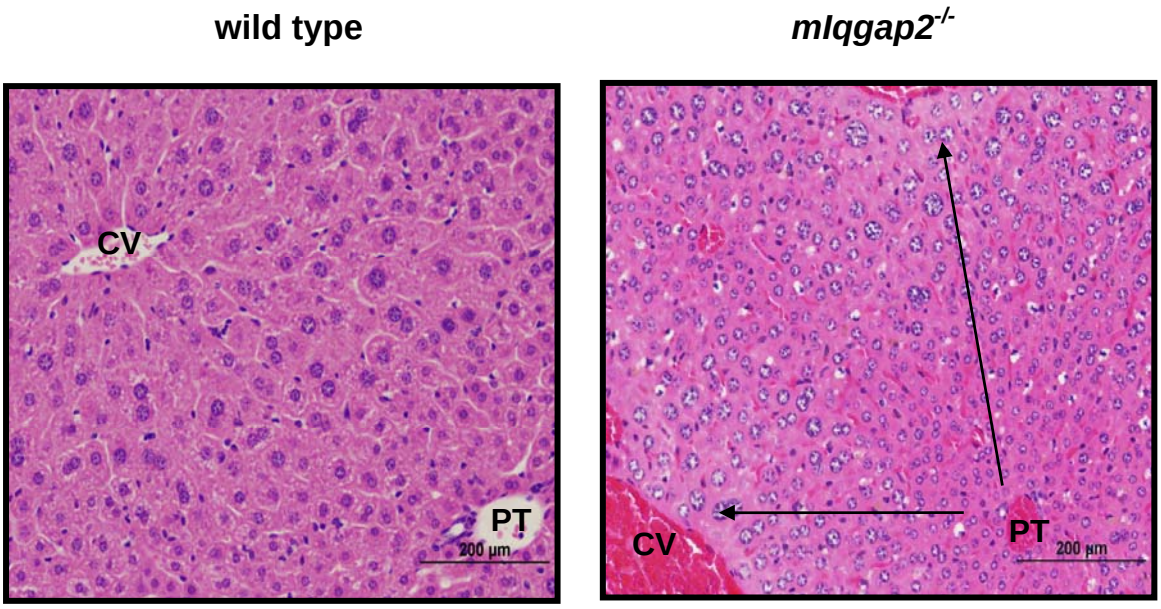

Figure 6: Age-dependent alteration in *mIqgap2*$^{-/-}$ hepatic nuclear morphology is suggestive of hypoxia and increased apoptosis. Eight-month wild type and *mIqgap2*$^{-/-}$ livers were isolated and fixed overnight in 10% neutral-buffered formalin. After embedding in paraffin, livers were sectioned at 5 μm and stained using Hematoxylin and Eosin. Arrow denotes direction of blood flow. PT= portal triad, CV = central vein. Scale bar = 200 μm.

homogenous in size. However, in *mIqgap2*$^{-/-}$ mice the smaller nuclei penetrate nearly 50% towards the central vein. Also, the morphology of the 2 populations of nuclei is much more heterogeneous. These observations are suggestive of hypoxia with implications regarding mitochondrial function. Interestingly, this gradient in 1 and 4 month *mIqgap2*$^{-/-}$ mice is indistinguishable from littermate controls (data not shown). Furthermore, a qualitative increase in apoptotic hepatocytes was observed in 8-month H&E sections. As a means of quantifying the observation of increased apoptosis, TUNEL staining was performed. No difference in 1 month mice was observed; however, a nonstatistical increase in 4 month mice was evident and a significant 5-fold increase in apoptotic hepatocytes at 8-months of age was observed (**Figure 7B**). To perform a second independent test which would correlate with the age-dependent increase in apoptotic bodies, biochemical analysis of blood serum was performed. A correlative increase in liver specific aspartate aminotransferase (AST) (**Figure 7A**) but not alanine aminotransferase (ALT), cholesterol, bilirubin, or high density lipoprotein (HDL) was observed (data not shown). This increase also was not due to any muscle damage as evidenced in creatine phosphokinase (CPK) levels (53.6 ± 6.3 U/L for wild type, 72.4 ± 20.59 U/L for *mIqgap2*$^{-/-}$ 8 months, n=5).

mIqgap2$^{-/-}$ hepatocyte mitochondria are structurally abnormal.

The age-dependent onset of hepatopathogenesis is characteristic of many mitochondrial disorders, attributed to the decline in oxidative phosphorylation capacity in mitochondria(135). Analyses of liver electron microscopy (EM)

Figure 7

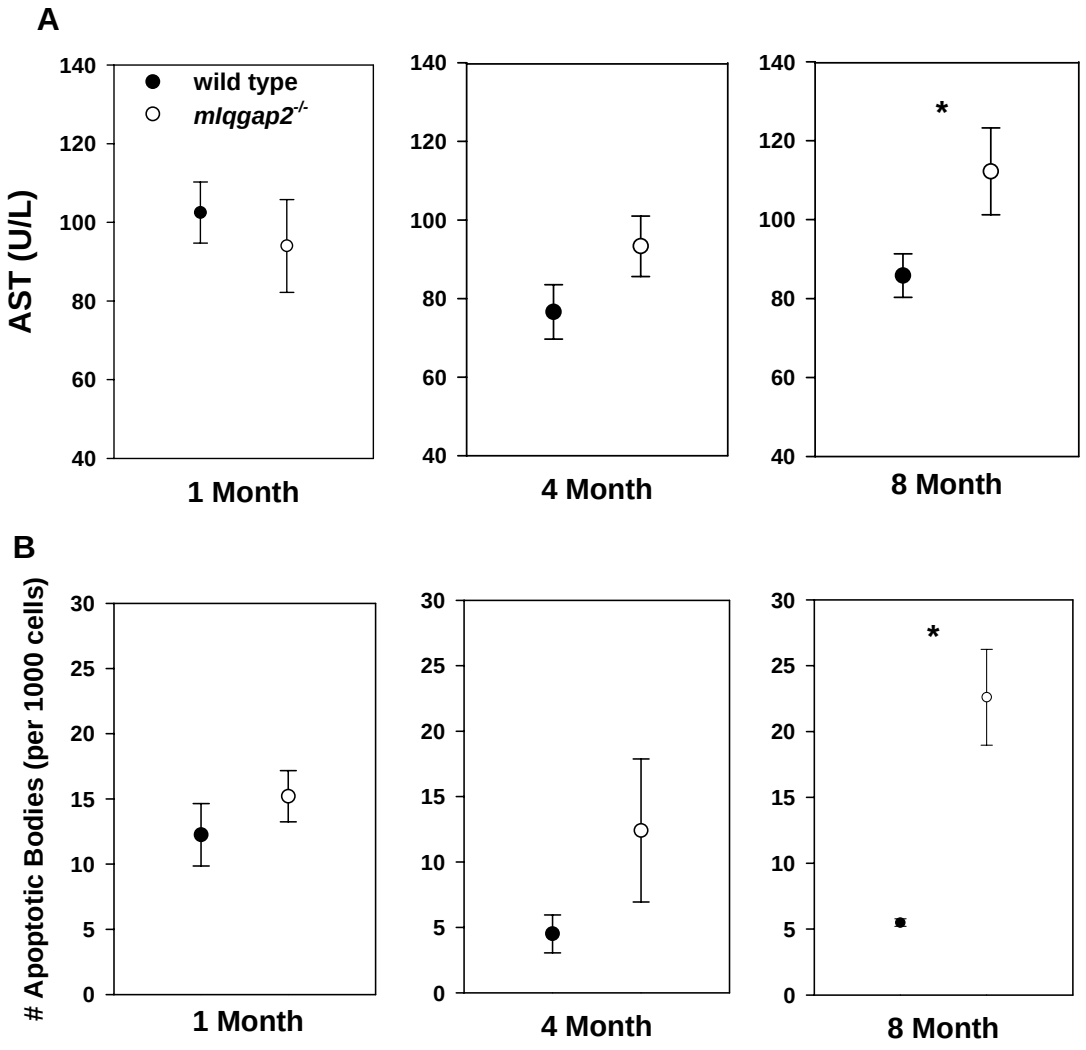
A
AST (U/L)
140
120
100
80
60
40
wild type
mlqgap2-/-
1 Month
4 Month
8 Month
*
B
Apoptotic Bodies (per 1000 cells)
30
25
20
15
10
5
0
1 Month
4 Month
8 Month
*

Figure 7: Age-dependent increase in liver AST correlates with the increase in apoptotic hepatocytes. (**A**) Blood was collected from retro-orbital bleeds of anesthetized 1, 4 and 8 month wild type and *mIqgap2*$^{-/-}$ mice. After clotting at 1 hour at 37^{O}C, blood was centrifuged to isolate serum which was analyzed for hepatospecific enzymes. (**B**) Livers from 1, 4, and 8 month mice were isolated and fixed in 10% neutral-buffered formalin overnight at 4^{O}C. After sectioning, tissues were subjected to TUNEL staining and scored for number of apoptotic hepatocytes (per 1000 cells). Data represents the mean ± SEM for n=10 mice for sera analysis and n=5 mice for TUNEL staining. Asterisk indicates $p<0.05$

sections and hepatic mitochondria structural integrity were performed. Ultrastructural analysis of hepatic mitochondria shows an age-dependent disruption of inner cristae structure, where 8 and 12 month *mIqgap2*$^{-/-}$ mitochondria display severe inner membrane disruption (**Figure 8A**), with no difference between 1 or 4 month wild type and *mIqgap2*$^{-/-}$ mitochondria. To assess if the structural defect affects mitochondrial integrity, mitochondria were isolated from liver tissue, loaded with tetramethyl rhaodamine ethyl ester (TMRE), and treated with calcium or valinomycin in a dose-dependent manner. Calcium is a specific effector of the Permablity Transition Pore (PTP, the complex regulating cytchrome c release as the primary signal for apoptosis)(27) (**Figure 8B**), while valinomycin is a potassium-dependent effector of the PTP (123) (**Figure 8C**). Flow cytometric analysis of 8-month wild type and *mIqgap2*$^{-/-}$ mitochondria reveals no disruption of membrane integrity, indicating that the altered mitochondrial structure is not attributed to the increased apoptosis observed in liver TUNEL sections. Parallel observations indicate that the mitochondrial abnormality is not associated with alterations in key mitochondrial proteins (cytochrome c, complexes I & II, and prohibitin)(112). Futher analysis of mitochondrial functional competency is pursued in detail in Section II of this manuscript.

Loss of IQGAP2 prevents *ex vivo* hepatocyte adhesion.

Further analysis of IQGAP2-deficiency necessitated *ex vivo* experimentation on hepatocytes. Qualitative observations of isolated primary

Figure 8

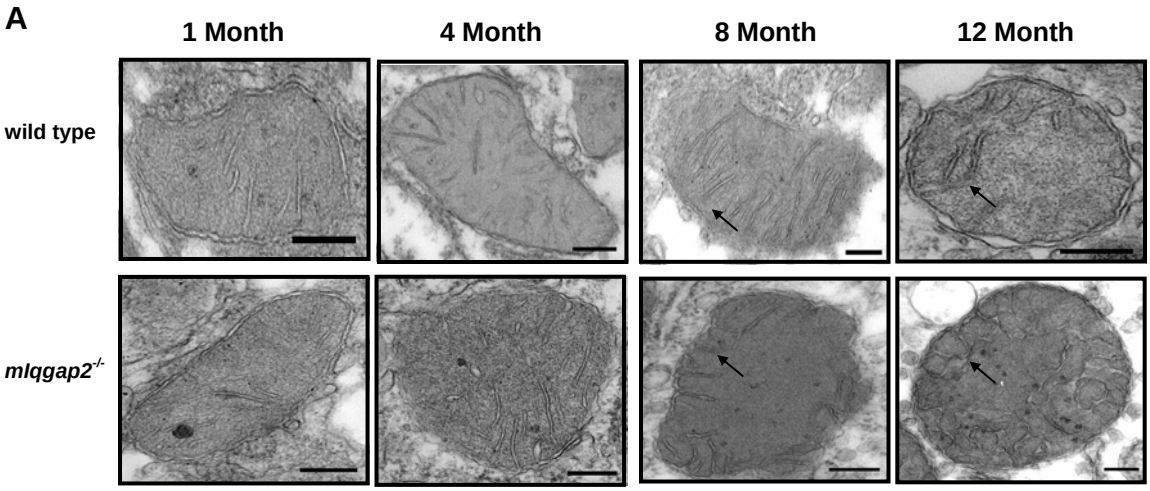
A
1 Month
4 Month
8 Month
12 Month
wild type
mlqgap2-/-

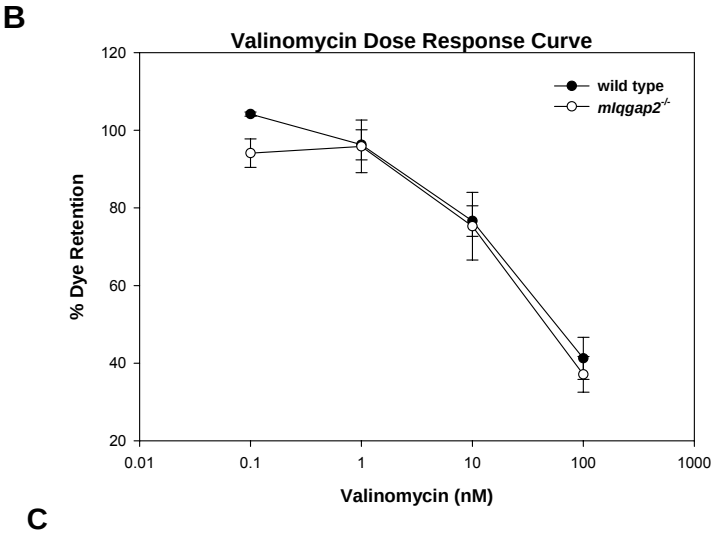
B
Valinomycin Dose Response Curve
wild type
mlqgap2-/-
% Dye Retention
120
100
80
60
40
20
0.01
0.1
1
10
100
1000
Valinomycin (nM)

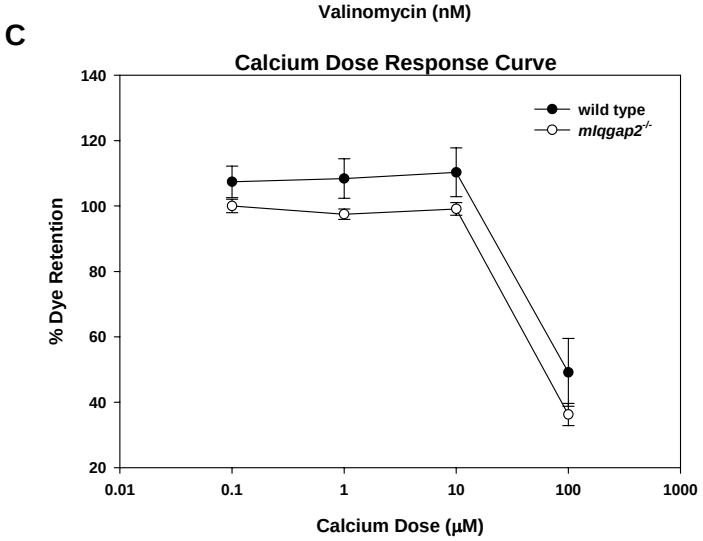
C
Calcium Dose Response Curve
wild type
mlqgap2-/-
% Dye Retention
140
120
100
80
60
40
20
0.01
0.1
1
10
100
1000
Calcium Dose (µM)

Figure 8: Abnormal mitochondrial morphology is not associated with the increased apoptosis observed in *mIqgap2*$^{-/-}$ hepatocytes. (**A**) Wild type and *mIqgap2*$^{-/-}$ livers from 1, 4, 8, and 12 month mice were isolated and fixed in EM fixative overnight at 4^{O}C. After mounting and sectioning, livers were subjected to electron microscopy to assess mitochondrial morphology. (**B & C**) Mitochondria from 8 month wild type and *mIqgap2*$^{-/-}$ livers were isolated by homogenization in isotonic buffer. Homogenates were subjected to differential centrifugation to isolate mitochondria. Hepatic mitochondria were loaded with 50 mM with calcium (concentrations in μM; **B**) or valinomycin (concentrations in nM; **C**) at concentrations of 0.1, 1, 10, or 100, respectively. After 10 minute incubation, mitochondria were subjected to flow cytometry and 10,000 gated events were counted. Data represent the mean ± SEM for n=5 mice per genotype. Arrows depict the normal (wild type) or abnormal (*mIqgap2*$^{-/-}$) inner cristae structure. Scale bar = 200 nm.

hepatocytes revealed *mIqgap2*$^{-/-}$ cells were not viable after 24 hours of incubation on type I collagen substrates. Quantitative assessment of this observation was performed by plating isolated hepatocytes on specific extracellular substrates and assaying for viability 24 hours post-incubation. Equal cell counts from different ages were placed on varying cell adhesion matricies, including type I collagen, fibrinogen, fibronectin, laminin, BSA and no coating. Viability was assessed using MTT based detection systems. After 24 hour incubation, nearly 10-fold less *mIqgap2*$^{-/-}$ hepatocytes was viable on any matrix at 1 and 4 months of age (**Figure 9A & B**). 8 month *mIqgap2*$^{-/-}$ hepatocytes are also decreased in viability (**Figure 9C**); however, 8 month wild type hepatocytes are not amenable to collagenase treatment, which is demonstrated by reduced levels of viability compared to 1 and 4 month wild type hepatocytes.

Figure 9

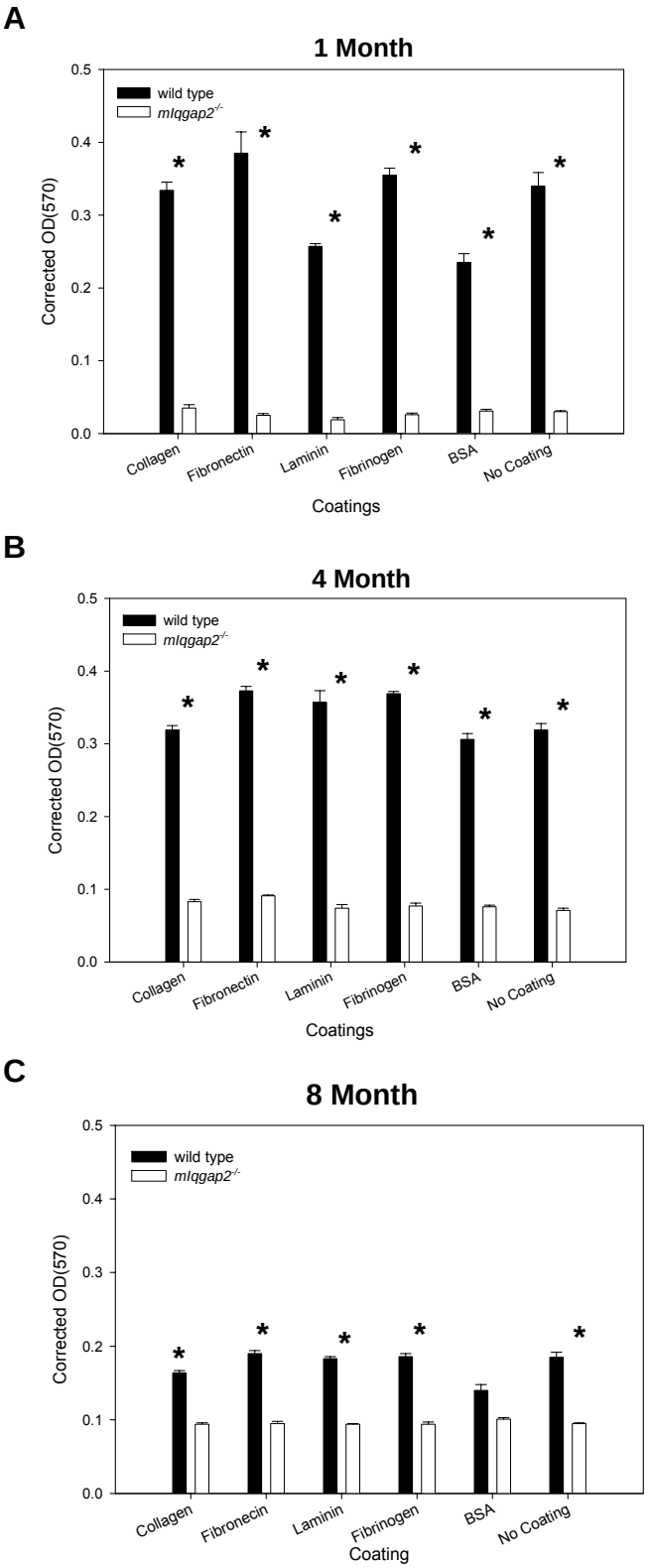
A
1 Month
wild type
mIqgap2-/-
Corrected OD(570)
0.0
0.1
0.2
0.3
0.4
0.5
Collagen
Fibronectin
Laminin
Fibrinogen
BSA
No Coating
Coatings
B
4 Month
wild type
mIqgap2-/-
Corrected OD(570)
0.0
0.1
0.2
0.3
0.4
0.5
Collagen
Fibronectin
Laminin
Fibrinogen
BSA
No Coating
Coatings
C
8 Month
wild type
mIqgap2-/-
Corrected OD(570)
0.0
0.1
0.2
0.3
0.4
0.5
Collagen
Fibronecin
Laminin
Fibrinogen
BSA
No Coating
Coating

Figure 9: *mIqgap2*$^{-/-}$ hepatocytes lack the capacity to adhere to extracellular matrices after collagenase treatment. Hepatocytes from 1 (**A**), 4 (**B**), or 8 (**C**) month mice were isolated by modified collagenase liver perfusion. Perfused livers were gently ruptured and centrifuged 3 times in Wash Buffer to remove cell debris. After isolation, $1x10^5$ cells were plated on either collagen, fibronectin, laminin, fibrinogen, BSA or no coating, and assessed for viability after 24 hour incubation using MTT based methodologies. Data is representative of 2 independent experiments and is the mean ± SEM for triplicate wells. Asterisk indicates $p<0.05$

Conclusions

Preneoplastic analysis of mIqgap2$^{-/-}$ mice suggests progression to cancer

The work presented here coupled with other work from our lab provide a physiologically relevant role for IQGAP2 in HCC. Analysis of preneoplastic mice reveals an age-dependent hepatopathy characterized by an increase in hepatospecific AST but not ALT with a correlative increase in apoptotic hepatocytes. A hallmark of preneoplasm in HCC is an increase in the proliferative/necrotic cycle in hepatocytes(45). Furthermore, the phasic progression of HCC involves a deregulated balance of cell stability in favor of hyperproliferation(43). While hepatocyte turnover in *mIqgap2*$^{-/-}$ livers remains unknown, based on the progressive increase of apoptotic hepatocytes measured, it is reasonable to assume that hepatocyte proliferation is increasing in parallel.

Observations of markers for hepatocarcinogenesis reveal that E-Cadherin is significantly downregulated in these neoplasms(107). No disruption in the expression level or subcellular localization of certain IQGAP2-binding partners such as E-Cadherin was observed at any age tested, suggesting the onset of HCC may occur after 8 months. More detailed analysis from our lab of *mIqgap2*$^{-/-}$ livers reveals that indeed, E-Cadherin expression is lost in microdissected tumors(112) in *mIqgap2*$^{-/-}$ mice older than 18 months.

Furthermore, 8-month *mIqgap2*$^{-/-}$ mice display an abnormal cellular gradient extending from the portal triad to the central vein. This is characterized by the disproportionate number and size of hepatic nuclei observed in *mIqgap2*$^{-/-}$ liver sections. This abnormal gradient is consistent with chronic hypoxic

conditions(28), suggesting either a depletion of oxygen in cells proximal to the central vein or a defect in mitochondrial function. Further investigation reveals an age-dependent increase in the disruption of *mIqgap2*$^{-/-}$ mitochondrial inner cristae structure to the exclusion of functional deficiencies related to apoptosis as shown by dose-dependent treatment with valinomycin or calcium. While these data contrast with prior experiments seen in mitochondrial diseases where an age-dependent reduction in the oxidative phosphorylation capability in hepatic mitochondria(135), it may indicate a novel IQGAP2-dependent mitochondria-related function (e.g. fatty acid metabolism) independent of the role of mitochondria in apoptosis.

To further understand the role of IQGAP2 in hepatocarcinogenesis, *ex vivo* experimentation was to be performed. In an effort to isolate hepatocytes we noted that *mIqgap2*$^{-/-}$ hepatocytes lack the ability to adhere to specific extracellular matrix substrates after collagenase treatment, suggesting either a loss of specific integrin expression related to extracellular matrix adhesion or the inability for hepatocytes to reorganize cytoskeletal elements in relation to adhesion. Inhibition of β1-integrin results in defective ex-vivo hepatocyte adhesion(105), which is independent of hepatocarcinogenic formation(136). This may suggest IQGAP2 associates with integrins in a novel pathway parallel to the established observation of IQGAP2 involvement in the canonical Wnt/Frizzled pathway.

The data presented here, in that the development of HCC is predated by a hepatic enzymopathy and mitochondrial damage, suggest that an associated

defect in mitochondrial β-oxidation and/or energy metabolism could be implicated in the subsequent malignant transformation. Accordingly, here we also utilize *mIqgap2*$^{-/-}$ mice to more rigorously dissect their altered fuel utilization.

II. IQGAP2-Dependent Role in Metabolic Switching

Background

Fuel Metabolism and Triglycerides

Triglyceride (TG) utilization exemplifies an evolutionary ability for higher organisms to adapt to differing sources of fuel. It serves as high density storage macromolecules during periods of feeding, formed from excessive dietary fatty acids (FA) and carbohydrates in the liver and adipose tissue via lipogenesis(108, 118). After feeding, insulin is the major hormone governing the regulation of carbohydrate and FA utilization(116). Glucose and amino acids stimulate insulin release from β-cells in the pancreas which targets the liver, muscle and adipose tissues to process glucose and FA for ATP production(**Figure 10**)(108). Muscle tissue will utilize nearly 20% of energy derived from serum glucose, as well as participate in glycogenesis for subsequent energy storage. In liver, insulin inhibits glycogenolysis via downregulation of glycogen phosphorylase and stimulates glycogenesis via upregulation of glycogen synthetase(57). In liver and adipose tissue, insulin also functions to promote *de novo* lipogenesis from glucose via enzymes such as ATP citrate lyase and acetyl-CoA carboxylase(55, 106). Subsequent TG synthesis from either *de novo* FA or dietary FA is less well understood. However, diacylglycerol acetyltransferases1 & 2 are known to be important for the formation of TG from diglycerides, possibly due to induction of the transcription factor sterol regulatory element binding protein-1c (SREBP-1c)(116).

Figure 10

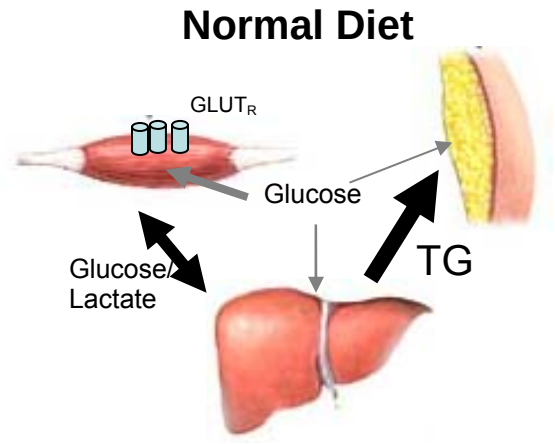
Normal Diet
GLUT$_R$
Glucose
Glucose/
Lactate
TG

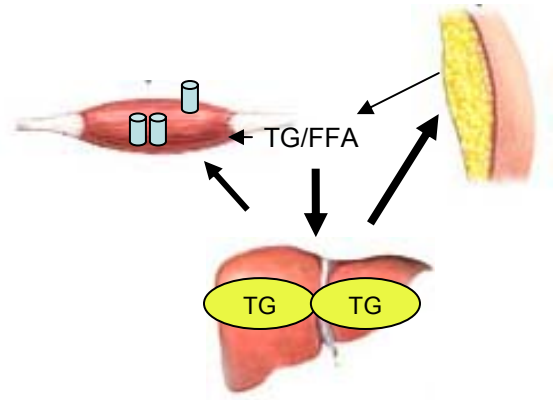
Fasting / High Fat Diet
TG/FFA
TG
TG

Figure 10: A representation of the utilization of glucose (Normal Diet) and fatty acids (Fasting/High Fat) and the interorgan crosstalk between the liver, muscle and adipose tissues. After feeding, the majority of serum glucose is taken up by skeletal muscle tissue via GLUT4 for immediate utilization or storage as intramuscular glycogen. Adipose tissue will take up minimal amounts of glucose for energy whereas the majority of glucose will participate in glycogen/TG synthesis. The liver also utilizes glucose, both for energy and conversion into glycogen for intrahepatic storage or TG synthesis which is either stored intrahepatically or exported for storage in adipose tissue. The Cori cycle occurs between muscle and liver tissues, where excess lactate is exported from muscle tissue to be processed back into glucose by liver tissue. In fasting or high fat diet conditions, cell surface levels of GLUT4 are minimized on muscle tissue and FA are metabolized by all three tissues. Muscle utilizes FA for energy, and adipose tissue (under fasting conditions) will release FA for peripheral tissue utilization or (under high fat conditions) will uptake FA for conversion into TG. The liver will process FA for peripheral tissue utilization as well as store excess FA in times of excess. Grey lines indicate glucose where black lines indicate FA. Width of line correlates to amount.

Figure 11

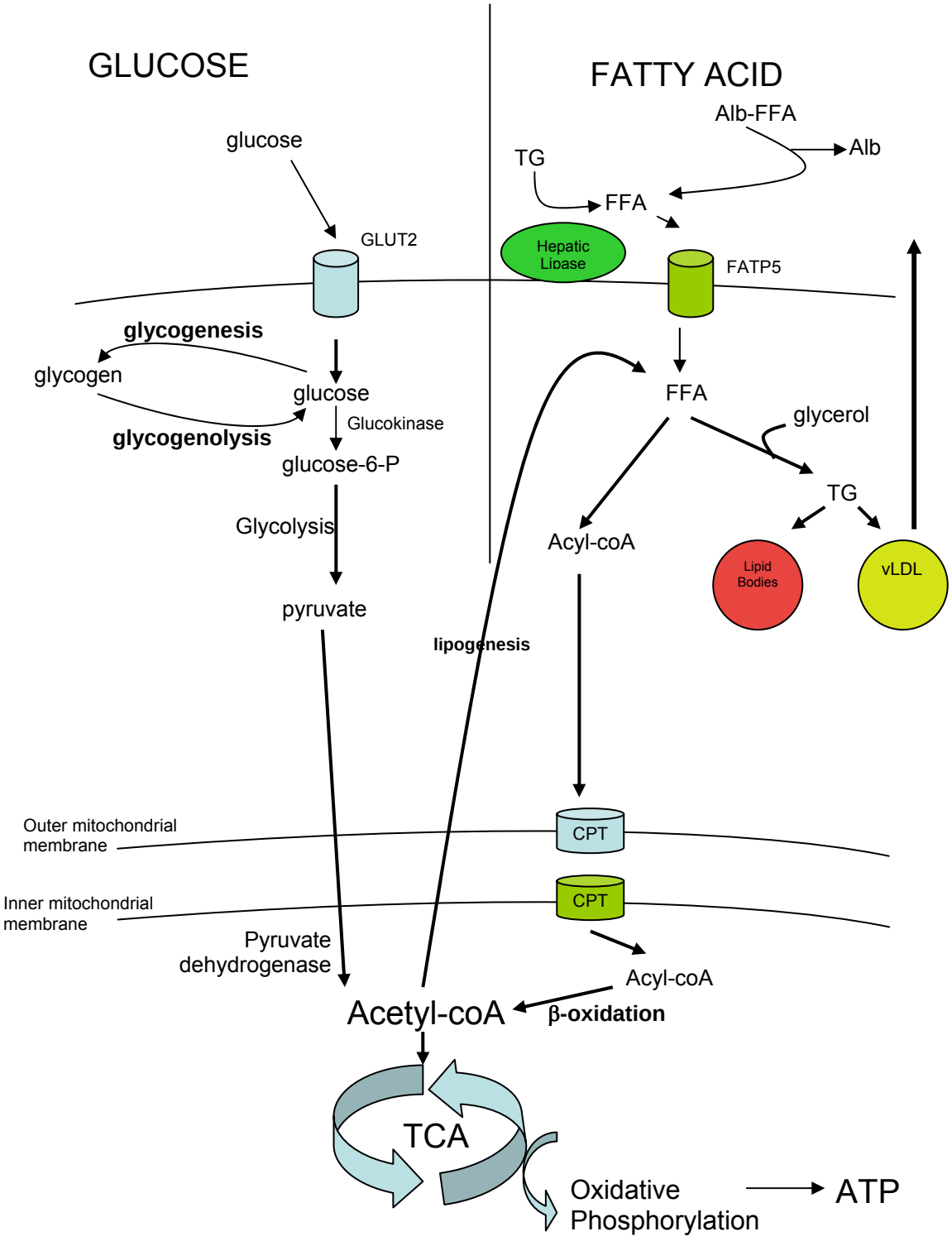
GLUCOSE
FATTY ACID
glucose
Alb-FFA
Alb
TG
FFA
GLUT2
Hepatic Lipase
FATP5
glycogenesis
glycogen
glucose
Glucokinase
glycogenolysis
glucose-6-P
FFA
glycerol
TG
Glycolysis
Acyl-coA
Lipid Bodies
vLDL
pyruvate
lipogenesis
Outer mitochondrial membrane
CPT
Inner mitochondrial membrane
CPT
Pyruvate dehydrogenase
Acyl-coA
Acetyl-coA
β-oxidation
TCA
Oxidative Phosphorylation
ATP

Figure 11: A schema depicting hepatic metabolism of glucose and fatty acids and the common convergence at the metabolic intermediate, acetyl-CoA. After feeding, glucose is taken up into hepatocytes via the facilitated glucose transporter, GLUT2. After transport, glucose is immediately phosphorylated to produce glucose-6-phosphate and subsequently metabolized into pyruvate via glycolysis. After transport, excess glucose is stored as the macromolecule glycogen. Pyruvate is then transported across the mitochondrial membranes, conjugated to Coenzyme-A (CoA) and dehydrogenated to form acetyl-CoA, the main input into the tricarboxylic acid cycle (TCA). Oxidative phosphorylation allows for the production of ATP from metabolic intermediates in the TCA cycle. FA are processed in hepatocytes after transport across the plasma membrane via the facilitated fatty acid transporter, FATP5. After transport, FA are conjugated to CoA to form acyl-CoA. Excess FA are resynthesized into TG and stored intrahepatically or coupled to apolipoproteins for export at low density lipoproteins (LDL) molecules. Acyl-CoA intermediates are transported into the mitochondria via carnitine palmitoyl transferases (CPTs). Intramitochondrial acyl-CoA intermediates are then reduced to numerous acetyl-CoA molecules via β-oxidation. Excess acetyl-CoA can be exported out of the mitochondria and resynthesized into FA via lipogenesis.

Conversely, during periods of fasting, insulin levels decrease and glucagon stimulates glycogenolysis in muscle and liver tissues; where muscle utilizes the glucose for energy, the liver supplies other critical peripheral tissues such as the brain with glucose as an energy supply (**Figure 10**). Adipose tissue is redirected to lypolysis where free fatty acids (FFA) are released into plasma for β-oxidation by various tissues, such as muscle and liver. (**Figure 11**)(108).

Hepatic Triglyceride Processing

The processing of TG in hepatocytes occurs in both the fed and fasted state, and occurs in three generalized stages (**Figure 11**). First, TG are broken down into FFA via hepatic lipase, and then uptake of FFA occurs via a saturatable, protein-mediated mechanism involving the fatty acid transport protein (FATP), FATP5(36), and to a lesser extent FATP2 and FAT/CD36(37, 49). Internalized FFA is either bound in its free form to fatty acid binding proteins (FABPs) or conjugated to Coenzyme-A (CoA) to form an acyl-CoA intermediate, which binds ACBP(20, 24). Interestingly, FATPs were recently discovered to harbor acyl-CoA synthetase activity(117), showing FATPs function not only to internalize FFA, but are also responsible for their conjugation to CoA. Depending on the organism's energetic state, internalized FFA will be (a) processed through β-oxidation for energy production or, (b) resynthesized into TG for intrahepatic storage or, (c) packaged into low density lipoprotein (LDL) molecules for secretion into plasma.

β-oxidation occurs in mitochondria, where FFA are conjugated to carnitine and transported across the mitochondrial membrane via carnitine

palmitoyltranslocases (CPT)(69). These acyl-CoA intermediates are then processed by β-oxidation to yield numerous 2-carbon acetyl-coA intermediates that enter the Krebs cycle to generate ATP. Perturbations in any of these stages result in imbalanced homeostasis, and can ultimately progress to disease(78).

Epidemiology and Etiology of Diabetes

It is becoming widely accepted that the inability for fuel flexibility leads to numerous prototypic, polygenic metabolic pathologies, such as obesity, type 2 diabetes, and metabolic syndrome(70, 78). Since the pathologies of these disorders are so juxtaposed, this overview will focus on the epidemiology and etiology of diabetes.

Diabetes is quickly becoming a leading cause of morbidity and mortality in many Western countries(2, 131). Annually, nearly 2.5 million deaths are attributed to diabetes(131). Without significant global attention and action, it is predicted that a 50% increase in diabetes-related deaths will occur within 10 years(2). Diabetes can be classified into 3 categories: type 1, type 2, and gestational diabetes.

Type 1 Diabetes

Type 1 diabetes, or insulin dependent diabetes mellitus (IDDM), is the result of polygenic disorders in glucose metabolism. Almost entirely a result of genetic defects, this form of diabetes requires daily insulin administration and is rapidly fatal in newborns and infants if not diagnosed(2). Classifications of type 1 diabetes categorize 18 different genetic loci (IDDM1 – IDDM18)(30, 72), although this method of classification is becoming outdated. This is due to the

lack of statistical significance needed from large studies to classify IDDM types based on certain candidate genes. IDDM1 genomically maps to the human leukocyte antigen region(96), which encodes genes coding for the major histocompatability complex. This form of type 1 diabetes generates autoantibodies targeted to β-cell islets in the pancreas. IDDM2 maps to the insulin gene, where many variable number tandem repeats have been identified(9, 99). IDDM2 – 18 compromise many monogenic traits that contribute to maturity onset diabetes of the young (MODY)(132). Genes implicated in MODY include hepatocyte nuclear factor-4, hepatic transcription factor-1 and -2, glucokinase, and insulin promoter factor-1(132).

Type 2 Diabetes

Type 2 diabetes (non-insulin dependent diabetes mellitus, NIDDM) accounts for 90% of all reported cases of diabetes(2, 131). Unlike type 1 diabetes, type 2 diabetes can arise from polygenic inherited traits, as well as numerous environmental factors. In fact, the rise in type 2 diabetes has a direct correlation to the increasing rates of obesity due to “Western” dieting and poor exercise habits(39). Diabetes is a progressive disease and minimal clinical observation is based on fasting glucose levels greater than 126 mg/dl and 2 hour postprandial glucose levels greater than 200 mg/dl(34). Failure to manage diabetes results in severe pathological complications including: morbid obesity, pancreatic β-cell destruction, retinopathy, blindness, heart disease, vascular damage of distal appendages resulting in amputation, and death(2).

Gestational Diabetes

Gestational diabetes is pathologically similar to the early stages of type 2 diabetes. In mild conditions it can be easily controlled with diet modification, mild exercise, and post partum weight loss. In mild to moderate cases of gestational diabetes, mothers revert to normalcy after birth, however, the susceptibility to type 2 diabetes increases 6-fold(114). More severe cases or poor management of gestational diabetes require supplemental insulin and neonatal monitoring. Unlike insulin, plasma glucose easily crosses the placental barrier where excessive fetal lipogenesis can result in macrosomia(2, 114). This condition presents numerous challenges, such as shoulder displacement during birth, and severe hypoglycemia, resulting in poor respiratory function. Genetic causes for gestational diabetes relate to genes implicated in MODY and type 2 diabetes, suggesting gestational diabetes is heavily influenced by environmental cues(114).

Treatments for Diabetes

Current treatments of diabetes at early stages in intervention include diet modification, exercise, and moderate weight loss. More advanced stages include subcutaneous insulin administration. Methods of self-administration involve calculation of postprandial glucose and injection of the appropriate amount of insulin. Recent advances have generated insulin pumps capable of constant infusion of steady amounts of insulin with bolus infusions possible after a meal or abnormally high glucose levels(2, 122). Patients with moderate to severe insulin resistance are given oral drugs such as sulfonylureas

or meglitinides (β-cell stimulators), thiazolidinediones (insulin sensitizer), or biguanides which are capable of halting hepatic glucose production. α-glucosidase inhibitors indirectly control glucose by decreasing the rate of starch breakdown. Patients are also capable of taking combinations of these drugs for a synergistic effect(111).

Murine Models Detailing Fuel Inflexibility and Diabetes

Numerous studies of mouse models for obesity and diabetes have pointed to the ability of tissues such as skeletal muscle, liver and adipose tissue to cross-talk to one another and modulate their affinities for certain fuels. Tissue specific knockout of the glucose transporter isoform 4 (GLUT4) (adipose and muscle GLUT4 knockout, AMG4KO)(75) led to the observation that increased hepatic lipid utilization compensates for the decreased adipose and muscle glucose utilization. Mice with muscle specific deletion of Protein Kinase C – λ (PKC-λ), an effector kinase of Akt and downstream of PI3K, display diabetic and metabolic syndromes characterized by glucose intolerance, systemic insulin resistance, abdominal obesity, steatohepatitis and hyperlipidemia(47). The inability for adipose and muscle GLUT4 knockout mice or muscle specific PKC$\lambda^{-/-}$ mice to effectively process glucose results in a shift in fuel selection to FA in these tissues, with a correlative increase in liver glucose uptake. Probably the most significant and thoroughly tested knockout model is of the insulin receptor (IR). Mice with total loss of IR quickly develop diabetes and die within 2 weeks of birth due to diabetic ketoacidosis(1). To better understand the pathological consequences of IR loss, investigators developed tissue specific IR knockouts.

Adipose-specific IR knockout mice lose total body fat and exhibit minimal serum TG, yet demonstrate no significant diabetic symptoms, suggesting adipose specific IR is not responsible for glucose homeostasis(12). Muscle-specific IR knockout mice are impaired in insulin-stimulated glucose transport, but are not systematically insulin-resistant or obese(21). However transgenic mice expressing dominant negative IR are severely insulin resistant, hyperinsulinemic, and lipotoxic due to increased serum FFA and TG, presumably due to increased lipogenesis(48). More so, normalcy can be achieved in these mice when treated with fibrate (a peroxisome proliferator activated receptor - α agonist) or phlorizin(48).

IQGAP2 and metabolic fuel switching

Here we utilize *mIqgap2*$^{-/-}$ mice to identify the role of IQGAP2 in metabolic fuel switching. *mIqgap2*$^{-/-}$ mice have increased metabolic rates, characterized by decreased respiratory quotients, activity levels, increased body fat composition and decreased basal glucose and triglyceride levels. Hepatic analysis of lipid processing indicates *mIqgap2*$^{-/-}$ hepatocytes have significantly increased TG export *in vitro*, which is also observed as the absence of steatosis during high fat diet conditions *in vivo*. More so, *mIqgap2*$^{-/-}$ skeletal tissue GLUT4 is unresponsive to fed conditions, suggesting a compensatory mechanism by muscle and fat tissue for the increased export of TG from hepatocytes. Taken together, the data presented clearly indicates the compensatory capability of peripheral tissues to utilize FA in *mIqgap2*$^{-/-}$ mice with implications in diabetes-like syndromes.

Materials and Methods

Body Weight and Food Consumption Monitoring

One, four, and eight month wild type and *mIqgap2*$^{-/-}$ mice were monitored for 2 weeks for body weight and food consumption by daily weighing.

Biochemical Analysis

Overnight fasted mice 4 months old were anesthetized using Metofane and bled by retro-orbital puncture. 200 μl of whole blood was allowed to clot at room temperature for 1 hour. Coagulated blood was spun at 14,000 x g for 5 minutes and serum removed. Levels of glucose and triglycerides were obtained using a MODULAR PP serum work area analyzer at Stony Brook University Hospital (Roche Diagnostics, Indianapolis, IN)(4).

Indirect Calorimetry Studies

Methodology was performed in collaboration with Jun Xu. Indirect calorimetry was performed on 4 mice per genotype at 1, 4 and 8 months of age as well as mice from the diet study. Mice were allowed to acclimate to new housing conditions for 24 hours. Oxygen consumption, carbon dioxide release and activity were simultaneously monitored for 3 day/night cycles using an Oxymax open circuit indirect calorimetry system (8 cage system) (Columbus Instruments, Columbus, OH). Instrument settings were: gas rate = 0.6 l/min; sample flow rate = 0.5 l/min; settle time = 120 s; measure time = 60 s. Results were analyzed for each 12-hour day / night cycle(8).

Fluorescent FA Uptake Studies

Freshly prepared hepatocytes were isolated from Metofane anesthetized mice 1, 4 and 8 months old using a modified *in situ* collagenase digestion of livers(73). Detailed methodology is described above in Section I: Material and Methods. For uptake analysis, 1 x 10^5 cells/well were incubated at 37^OC for 30 minutes followed by the addition of an equal volume of BODIPY-FA analog coupled to a novel quencher compound, Q-Red.1 (Molecular Devices, Sunnyvale, CA)(83). Readings were performed immediately after the addition of the FA compound in a Molecular Devices FLEX Station and analyzed using SoftMaxPro software(4).

FA Uptake and Oxidation Assays in Cultured Cells

Subcultured COS-1 cells at 50 – 60% confluence were transfected with pcDNA3.1+ (empty control) or J3Ω (IQGAP2-HA construct, gift of Dr. A. Bernards, Harvard University) using Lipofectamine LTX and Plus reagent (Invitrogen). The following day, transfected cells were split in triplicate into either 12-well plates for FA uptake or 96-well plates for FA oxidation assays. To assess for FA uptake, a modified uptake procedure was used(40). On the day of experimentation, cells were washed twice with PBS and serum starved with DMEM / low glucose for 60 minutes at 37^OC. Following serum starvation, cells were incubated at 37^OC for t=0.5, 1, 3, 5, 10, and 15 minutes with 125 μl of FAU solution (600 μM [^{14}C]-palmitic acid (1.4 μCi/mmol) and 120 μM FA-free BSA in

PBS). Following incubation, cells were washed 3 times with ice cold PBS, lysed with 500 μl lysis buffer (10mM Tris, 150mM NaCl, 1% NP-40 with protease inhibitors) and 400 μl aliquots used for scintillation counting; 100 μl was reserved for protein quantification. Cells were randomly sampled by immunoblotting for confirmation of transfection.

For FA oxidation, a 96-well apparatus designed by Abbott Labs(128) was used. Briefly, cells were serum starved for 1 hour in DMEM / low glucose and then incubated in FAO solution (600 μM [^{14}C]-palmitic acid (55 μCi/mmol), 120 μM FA-free BSA in PBS) for t=1, 5, 15, 30, 60 or 180 minutes. After incubation, 200 μl of 1M HCl was added to the cells, with the adjacent well containing 300 μl of 1M NaOH. Following an overnight incubation to capture CO_2, the 1M NaOH was quantified for [^{14}C]-CO_2 by scintillation counting.

Triglyceride Output Assay

HepG2 hepatoma cells plated at 50 – 60% confluency were transfected with siRNA targeted against either IQGAP2 (equimolar amounts of sense5'-ggAAUUCAggAAAUAUUUCTT and sense5'-gCAAAAUAggUggUAUUCUTT) or scrambled RNA (Ambion cat# 4605) using RNAiMax transfection reagent (Invitrogen). 48 hours post-transfection, cells were washed 2x with PBS and incubated for 3 hours at 37^{O}C with 0.5 μCi of [^{14}C]-oleic acid in serum free DMEM followed by a 4-hour chase with PBS and 0.05% FA-free BSA(129). Supernatants were collected and neutral fats isolated(50). Lipids were separated using Thin Layer Chromotography (TLC) with unlabeled tripalmitin as an external

reference. TG spots were scraped into 5 ml scintillation counting solution and counted. In parallel, cells were lysed in lysis solution (10mM Tris, 150mM NaCl, 1% NP-40 with protease inhibitors) and immunoblotted to ensure knockdown of IQGAP2.

Immunoblotting of Lysates

Either freshly isolated liver and muscle tissues or washed HepG2 cells were lysed in lysis solution (10mM Tris, 150mM NaCl, 1% NP-40 with protease inhibitors) and incubated on ice for 15 minutes. Tissues were homogenized in a Dounce homogenizer (30 strokes). Insoluble debris was centrifuged at 14,000 x g for 10 minutes. Protein quantification was performed according to manufacturer's directions (Pierce). 10 μg of lysate was electrophoretically separated and immunoblotted for either IQGAP2 (1:1000, Upstate), GLUT4 (1:1000, Cell Signaling Technologies), or GAPDH (1:2000, BD Biosciences) followed by incubation with HRP-conjugated secondary antibody and detected using enhanced luminosity (Pierce)(4).

Diet Modification Studies

Diet studies were completed using 16-week old male mice that were housed in a full-barrier facility with a 12-hour light/dark cycle and given full access to food and water unless otherwise stated. Mice of a single genotype (wild type or *mIqgap2*$^{-/-}$) were caged together to ensure standardization during all diet modification studies. Mice were weaned onto fixed diets over a 1-week

period (control chow diet contained 10% calories from fat, high fat diet contained 45% calories from fat; Research Diets, New Brunswick, NJ) prior to the beginning of the 6 week study. Diets were provided *ad libitum* (and intake carefully monitored) for 6 weeks prior to termination of studies, at which point mice were weighed and sacrificed for blood and organ processing; fat was quantified from epididymal fat pads.

Lipid Histochemistry

Wild type or *mIqgap2*$^{-/-}$ mice subjected to the high fat diet modification study were sacrificed under Metofane anesthesia and livers immediately submerged in cryosectioning solution (OCT compound, Sakura FineTek, Torrence, CA) and frozen at -80^{O}C overnight. Tissues were sectioned at 8 μm. Lipid staining was accomplished using Oil Red O staining on liver sections and was performed at Stony Brook University Hospital Histology Laboratory and analyzed for gross morphology.

Tissue Triglyceride Quantification

Upon completion of diet modification studies, mice were sacrificed under Metofane anesthesia, and livers removed. Livers were homogenized by Dounce homogenization (25 strokes) in PBS with 0.1 mM PMSF and 10 μg/ml leupeptin/aprotinin. 100 μl of liver homogenate was removed for protein quantification via standard BCA assay. Liver homogenates were mixed with 2 volumes of chloroform:methanol:sulfuric acid (2:1:0.5%)(22) and shaken for 2

minutes. After brief spinning to separate phases, the organic (lower) phase was removed and dried under nitrogen at 37^{O}C. The extract was then resuspended in 200 μl of 2% Triton-X 100. TG was quantified using Serum Triglyceride Determination Kit (Sigma, St. Louis, MO). To quantitate true TG content, 0.8 ml Free Glycerol Reagent was mixed with 10 ml sample and incubated 5 min at 37^{O}C. Samples were read at 540 nm in a standard spectrophotometer to obtain initial absorbance (IA). 0.2 ml of Triglyceride Reagent was then added to the sample and incubated 5 min at 37^{O}C. Samples were then read at 540 nm to obtain final absorbance(FA). To calculate true TG content:

$$\frac{(FA_{sample} - (IA_{sample} \times 0.80)}{(FA_{standard} - (IA_{blank} \times 0.80)} \quad X \quad [Standard]$$

Glucose Tolerance Testing and Insulin Measurement

Data and methodology (133) provided by Jun Xu. Mice were fasted overnight and allowed free access to water. 4 month wild type and *mIqgap2*$^{-/-}$ mice (n=3 per genotype) were bled prior to injection to establish baseline glucose levels. [1,2-$^{13}C_2$]Glucose was administered at 1mg glucose / g body weight via intraperitoneal injection. Blood samples were acquired via retro-orbital bleeding at t=0, 0.5, 1, and 2 hours post-injection. Glucose was determined by COBAS MIRA analyzer (Roche) and insulin levels determined by ELISA measurement(Crystal Chem, Downers Grove, IL).

Statistical Analysis

Results are expressed as the mean ± SEM of appropriate replicates and normalized to protein concentration where necessary. P values are calculated using unpaired Student's t-test, with $p<0.05$ considered statistically significant.

Results

mIqgap2$^{-/-}$ mouse basal metabolic differences suggest altered FA utilization.

Previous studies using IQGAP2 knockout mice revealed the hepatocyte restricted phenotype that occurred in an age-dependent manner(112). Also, age-dependent hepatospecific enzymes and mitochondrial structural studies in preneoplastic *mIqgap2*$^{-/-}$ mice suggested possible defects in function related to β-oxidation and energy utilization. To evaluate this, we initially employed indirect calorimetry to assess for metabolic defects. Interestingly, although there is no difference in VO_2 consumption (data not shown), *mIqgap2*$^{-/-}$ mice display a decrease in both their respiratory exchange ratio (RER) and activity at 4 months of age during both the diurnal and nocturnal cycle (**Table I**, **Figure 12A**). A theoretical maximum RER of 1.0 signifies glucose as a preferred fuel where a theoretical minimum RER of 0.75 signifies FA as the fuel. The RER of 1 month mice is slightly decreased in the nocturnal phase, whereas 8 month mice RER is defective in both diurnal and nocturnal phases, with a significant difference in nocturnal activity. (**Figure 12A**). This age-dependent decrease in RER and activity gives rise to the possibility of altered FA metabolism as well as overall higher metabolic activity in *mIqgap2*$^{-/-}$ mice.

To further dissect the decrease in RER and activity, food intake and body weight were monitored over 2 weeks for 1, 4 and 8 month mice. Interestingly, wild type and *mIqgap2*$^{-/-}$ mice display similar body weights at 1 and 8 months of age, yet *mIqgap2*$^{-/-}$ mice are ~13% lighter at 4 months. More so, 1 and 4 month

Figure 12

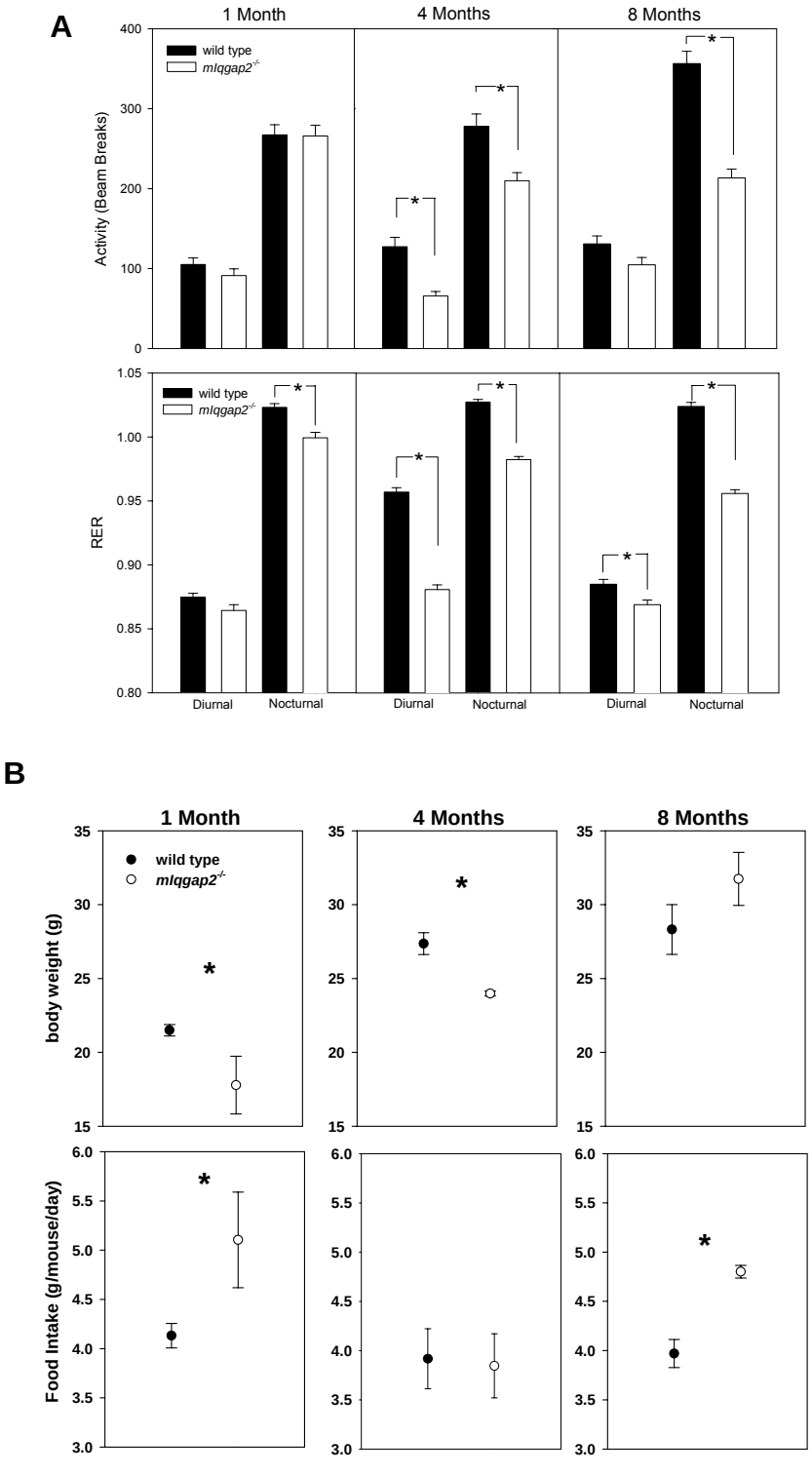
A
1 Month
4 Months
8 Months
wild type
mlqgap2-/-
Activity (Beam Breaks)
RER
Diurnal
Nocturnal
B
1 Month
4 Months
8 Months
wild type
mlqgap2-/-
body weight (g)
Food Intake (g/mouse/day)

Figure 12: *mIqgap2*$^{-/-}$ mice are metabolically more active than wild type. (**A**) Wild type and *mIqgap2*$^{-/}$ mice, ages 1, 4, and 8 months, were subjected to indirect calorimetry for 72 hours to assess VO_2 consumption, VCO_2 release, and activity levels. (**B**) Weekly monitoring of body weights and food consumption of the same set of mice as in **A**. Data is mean ± SEM for n=4 mice for indirect calorimetry and n=5 for food and body weight monitoring. Asterisk indicates $p<0.05$

Table I: Basal characteristics of 4 month wild type and *mlqgap2*$^{-/-}$ mice.

Parameter	*wild type*	*mlqgap2*$^{-/-}$	*p value*
Food Intake * (g/mouse/day)	3.92 ± 0.305	3.85 ± 0.33	N.S.
Body Weight (g) *	27.36 ± 0.74	23.98 ± 0.17	p<0.005
Body Fat (%)*	11.74 ± 0.72	15.28 ± 0.61	p<0.005
Glucose (mg/dl) §	151.00 ± 6.38	121.20 ± 13.96	p<0.05
Triglycerides (mg/dl) §	100.67 ± 14.05	54.00 ± 7.20	p<0.005
Insulin (μg/l) †	0.42 ± 0.21	0.61 ± 0.07	N.S.
Diurnal RER ‡	0.96 ± 0.003	0.88 ± 0.003	p<0.005
Noct. RER ‡	1.03 ± 0.002	0.98 ± 0.002	p<0.005
Diurnal Act (beam breaks) ‡	127.40 ± 11.53	65.61 ± 5.82	p<0.005
Noct. Activity (beam breaks) ‡	277.90 ± 15.46	209.89 ± 10.11	p<0.005

Values are mean ± SEM.
*,n=5
†, n=3
‡, n=4
§, n=6

mice consume similar amounts of food, whereas 8 month mice consume 25% more chow (**Figure 12B**). However, comparison of food intake to body weight reveals an age-dependent decrease in food consumption, reinforcing the possibility of increased metabolic rates from indirect calorimetry studies at younger ages.

Based on these data, prior data from studies of preneoplastic states of hepatocellular carcinoma, and the observation that *mIqgap2*$^{-/-}$ mice have a higher mortality rate at six months compare to wild type(112), 4 month mice were chosen for all subsequent studies. More detailed metabolic studies on 4 month mice reveal *mIqgap2*$^{-/-}$ mice have greater body fat composition as compared to littermate controls (**Table I**). More so, fasting serum glucose and TG display 20% and 45% decrease over wild type, respectively (**Table I**). Taken together, these data strongly suggest the possibility of altered FA / glucose utilization in *mIqgap2*$^{-/-}$ mice and were pursued in more detail.

Isolated hepatocytes are defective in immediate stages of FA uptake.

Given the role of IQGAP2 as a scaffolding protein capable of integrating cellular signals at the cell surface(18), and that *mIqgap2*$^{-/-}$ mice display hepatospecific mitochondrial abnormalities possibly related to metabolic function(112), we wished to delineate any abnormalities in FA uptake or FA oxidation. Accordingly, the quantification of FA uptake was performed on collagenase-isolated hepatocytes in real time using a fluorescent-based FA analog(83). Interestingly, *mIqgap2*$^{-/-}$ mice display a defect in the immediate

Figure 13

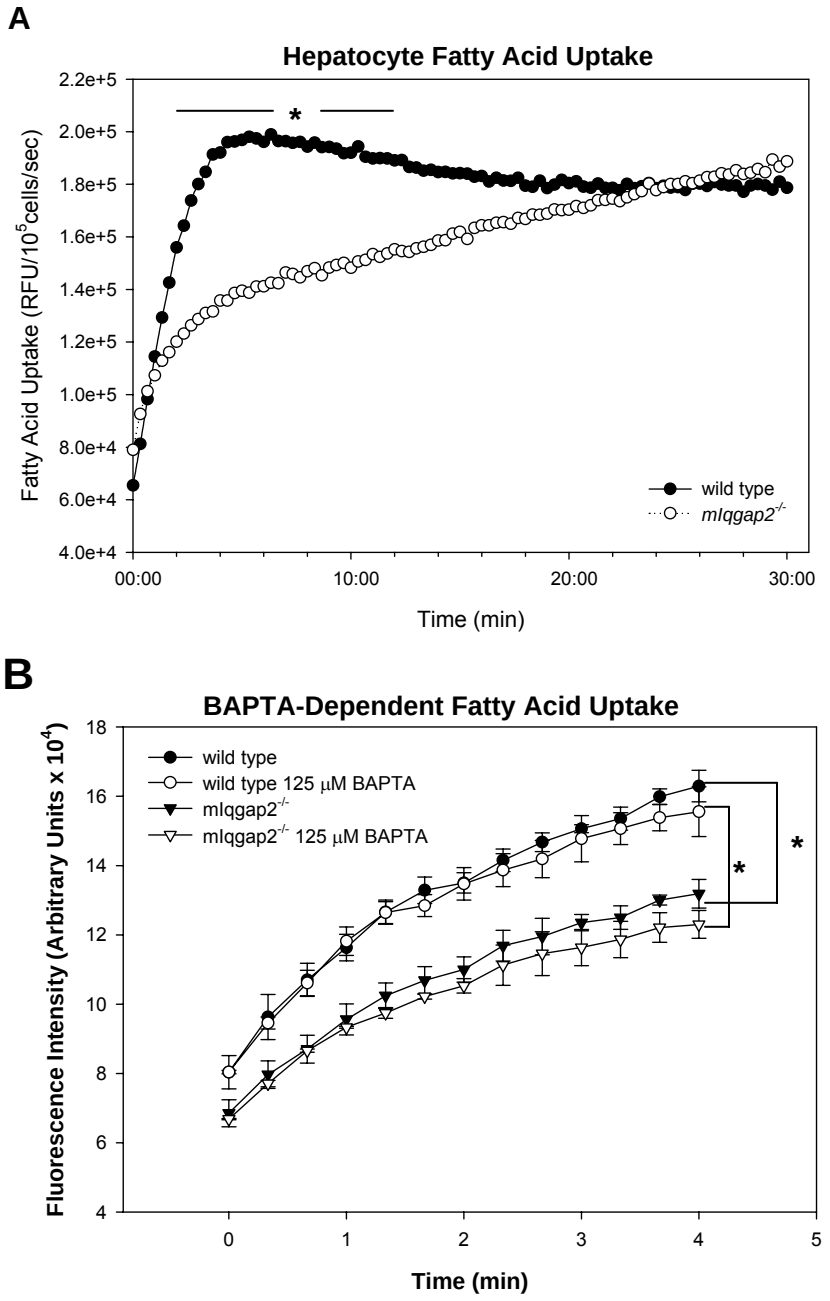
A
Hepatocyte Fatty Acid Uptake
Fatty Acid Uptake (RFU/10^5cells/sec)
2.2e+5
2.0e+5
1.8e+5
1.6e+5
1.4e+5
1.2e+5
1.0e+5
8.0e+4
6.0e+4
4.0e+4
*
00:00
10:00
20:00
30:00
Time (min)
wild type
mIqgap2-/-
B
BAPTA-Dependent Fatty Acid Uptake
Fluorescence Intensity (Arbitrary Units x 10^4)
18
16
14
12
10
8
6
4
wild type
wild type 125 μM BAPTA
mIqgap2-/-
mIqgap2-/- 125 μM BAPTA
*
*
0
1
2
3
4
5
Time (min)

Figure 13: *mIqgap2*$^{-/-}$ hepatocyte FA uptake is attenuated in the immediate-early stages and is not mediated by calcium. Livers from 4 month wild type and *mIqgap2*$^{-/-}$ mice were collagenase treated and livers removed. After gentle disruption to liberate hepatocytes, cells were centrifuged 3 times in Wash buffer to remove cell debris. $1x10^5$ cells were serum starved for 1 hour prior to incubation with BODIPY-FA and subjected to semi-quantitative real time fluorescent FA uptake analysis on a FLEXStation without (**A**) or with (**B**) 125 μM BAPTA. Data is representative of 3 independent experiments and is expressed as mean ± SEM for triplicate wells. Error bars are removed in **A** for clarity. Asterisk = $p<0.05$

stages of FA uptake (**Figure 13A**). This defect was evident among all ages tested, with the most pronounced defect occurring at 4 months of age (86% reduction in V_{max}) (**Table II**). Despite these immediate changes, FA uptake was indistinguishable at 12-15 minutes post-incubation (**Figure 13A**), which is recapitulated in tissue FA uptake at 10 and 30 minute time points (data not shown). Since calcium is a rapid inducer of intracellular events, coupled with the fact that IQGAPs are regulated by calcium binding to calmodulin motifs(80), we retested these events in the presence and absence of the calcium chelating agent, 1,2-bis(o-aminophenoxy)ethane-N,N,N',N'-tetraacetic acid (BAPTA). (**Figure 13B**). No evidence for calcium as a modulator for FA uptake was observed over 5 minutes. Furthermore, other work from our lab indicates that hepatic β-oxidation is not diminished in *mIqgap2*$^{-/-}$ mice (data not shown). Based on basal body fat composition, calorimetric data, and the lack of a defect in hepatic FA metabolism (uptake and β-oxidation), this would suggest the possibility that hepatic TG packaging and secretion is perturbed, in which case peripheral tissues could compensate for this defect.

IQGAP2 is not sufficient to increase uptake of FA or rates of oxidation, but is essential for TG partitioning *in vitro*.

To determine if IQGAP2 is sufficient to induce an increase in FA uptake or fatty acid oxidation, we transfected COS-1, cells with minimal ability to process FA (unpublished observations), with full length IQGAP2. Cells treated with a palmitate:BSA complex for time points from 30s – 4 hours show no difference in

Table II: Fatty acid uptake V_{max} values for 1, 4, and 8 month wild type and *mIqgap2*$^{-/-}$ mice

Age	*Genotype*	*V_{max} (RFU/10^5cells/sec)*	*P value*
1Month	Wild type	**1091.10 ±30.89**	$p < 0.05$
	mIqgap2$^{-/-}$	**921.98± 36.77**	
4 Months	Wild type	**809.26± 97.02**	$p < 0.005$
	mIqgap2$^{-/-}$	**121.31 ± 15.96**	
8 Months	Wild type	**1106.82 ± 87.97**	$p < 0.005$
	mIqgap2$^{-/-}$	**596.28 ± 38.57**	

Data is representative of 2 independent experiments. Values are mean ± SEM of triplicate wells.

either the rate of uptake (<5min) or the overall amounts of radiolabeled palmitate over 4 hours. Introduction of CD36 / FAT with IQGAP2 does not change the amount of FA uptake over similar time courses (**Figure 14A**). Furthermore, levels of FA oxidation are not altered over a 3 hour incubation (**Figure 14B**). This data reveals that IQGAP2 is not sufficient to increase FA uptake or oxidation in non-FA metabolizing cells.

Based on the understanding of the uptake and processing of FA and since *mIqgap2*$^{-/-}$ mice display a decrease in the immediate stages of FA uptake, but achieve the same steady state as wild type, and that wild type and *mIqgap2*$^{-/-}$ liver tissues show similar FA oxidation levels, we hypothesized that hepatocytes have increased TG secretion. To test this *in vitro*, human hepatoma cells were transfected with siRNAs against IQGAP2, treated with radiolabeled oleate, and assayed for TG secretion. After a three hour treatment with oleic acid, cells depleted of IQGAP2 display nearly a 6-fold increase in TG output (**Figure 15**).

mIqgap2$^{-/-}$ mice are protected from steatosis when challenged with high fat.

To utilize a second independent test to reinforce the *ex vivo* and *in vitro* observations of partly diminished uptake and increased TG secretion, we challenged mice using diet modification. 4 month wild type and *mIqgap2*$^{-/-}$ mice were placed on either a control (10% fat) or high fat chow (45% fat) diet. Upon completion of the 6 week diet, mice were sacrificed to assess body weight, and epididymal fat content. While wild type and *mIqgap2*$^{-/-}$ mice share comparable

Figure 14

A

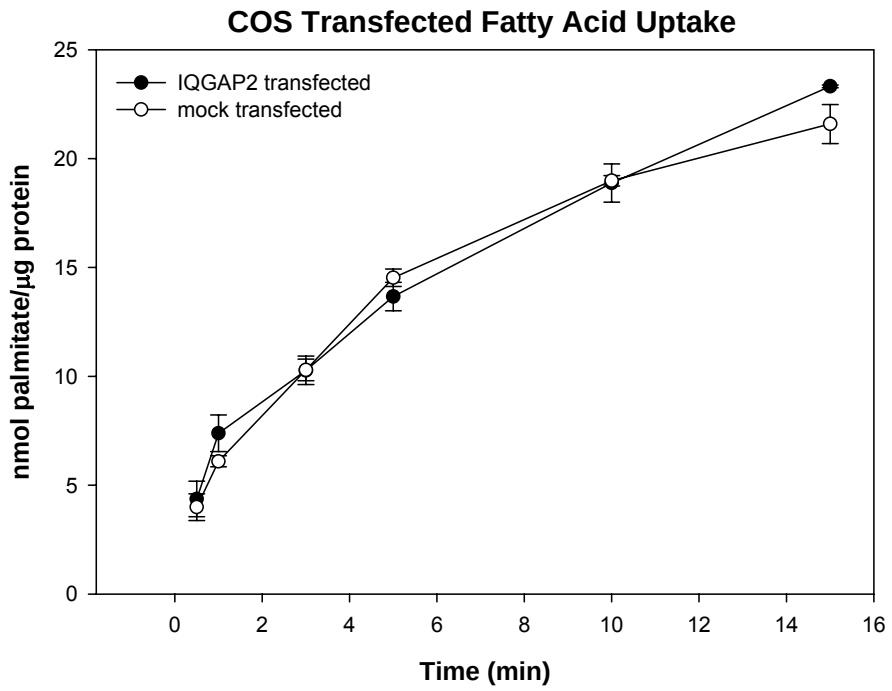
COS Transfected Fatty Acid Uptake
IQGAP2 transfected
mock transfected
nmol palmitate/µg protein
Time (min)
0
5
10
15
20
25
0
2
4
6
8
10
12
14
16

B

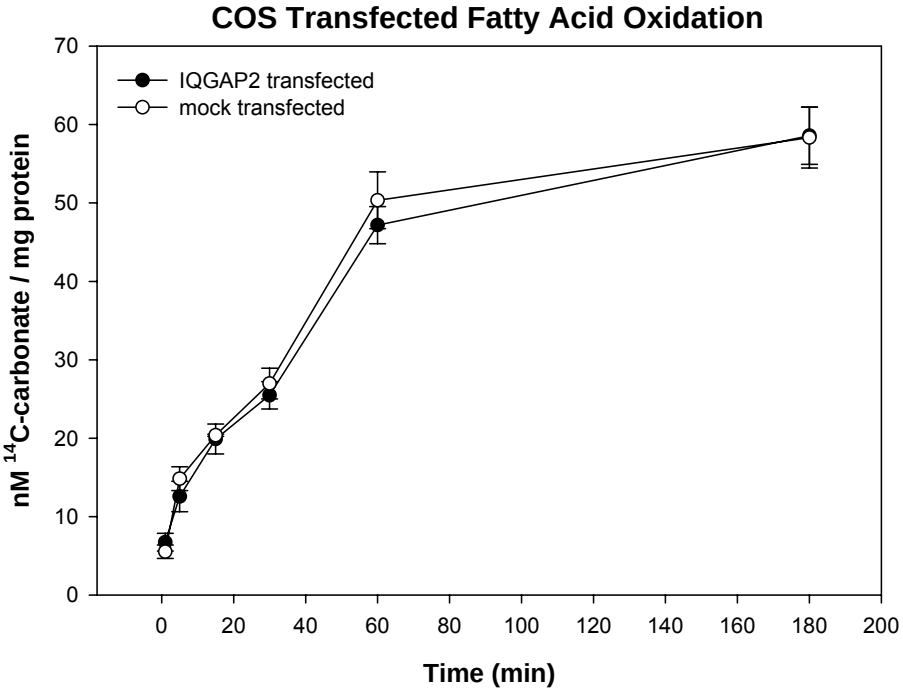
COS Transfected Fatty Acid Oxidation
IQGAP2 transfected
mock transfected
nM 14C-carbonate / mg protein
Time (min)
0
10
20
30
40
50
60
70
0
20
40
60
80
100
120
140
160
180
200

Figure 14: Neither FA uptake nor oxidation is modulated by IQGAP2 *in vitro*. COS cells were seeded at 50-60% the day before transfection. Cells were either transfected with pcDNA3.1+ (closed circles) or with IQGAP2-HA (open circles). The following day, cells were split in triplicate into 12 well dishes and incubated overnight. On the day of experimentation, (**A**) cells were serum starved for 60 minutes and then treated with 600 μM [^{14}C]-palmitate (1.4 μCi/mmol) and 120 μM BSA in PBS to assess FA uptake for times t= 0.5, 1, 3, 5, 10, or 15 minutes. (**B**) Similarly transfected cells were also split in triplicate wells of a 96 well plate the day before experimentation. To assess FA oxidation, cells were serum starved for 60 minutes and then plates were placed in the oxidation apparatus and incubated with 600 μM [^{14}C]-palmitate (1.4 μCi/mmol) and 120 μM BSA in PBS for times t=1, 5, 15, 30, 60, or 180 minutes. Following incubation, wells containing cells were treated with 1M HCl with 1M NaOH added to the adjacent well. After an overnight incubation to capture liberated CO_2, the NaOH was removed and counted by scintillation counting. Cells were assayed for protein content after assaying. Representative data of 3 independent experiments. Values are mean ± SEM for triplicate wells.

Figure 15

A

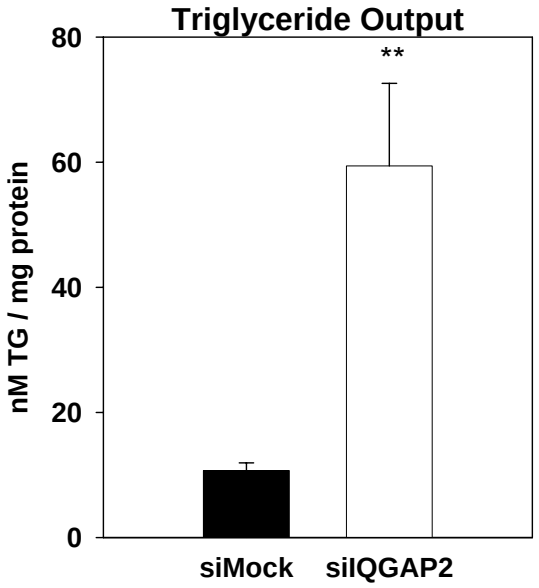
Triglyceride Output
nM TG / mg protein
80
60
40
20
0
**
siMock
siIQGAP2

B

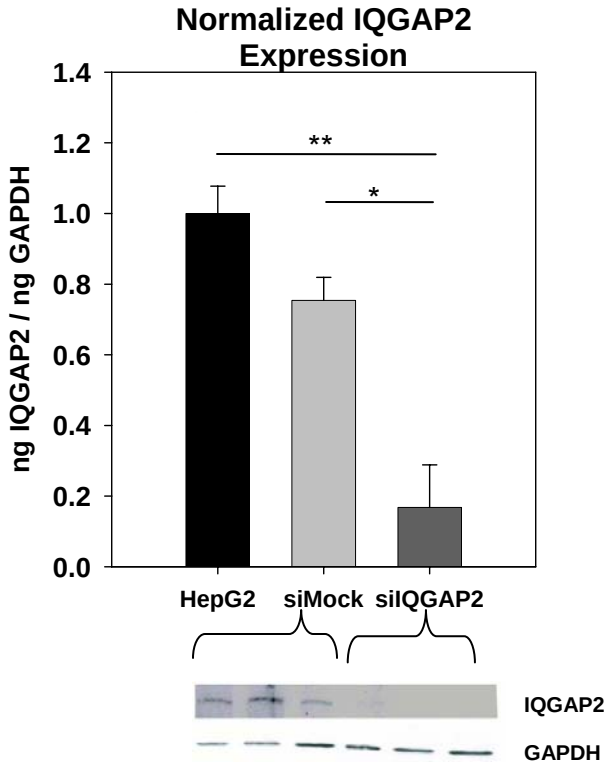
Normalized IQGAP2 Expression
ng IQGAP2 / ng GAPDH
1.4
1.2
1.0
0.8
0.6
0.4
0.2
0.0
**
*
HepG2
siMock
siIQGAP2
IQGAP2
GAPDH

Figure 15: Loss of IQGAP2 results in increased TG secretion *in vitro*. (**A**)HepG2 cells plated at 40-50% confluceny were transfected with scrambled siRNA or *Iqgap2* siRNA using RNAiMAX. 48 hour post-transfection, cells were washed three times with PBS and then incubated for 3 hours with 0.5 μCi of [^{14}C]-oleic acid in serum-free DMEM followed by a 4-hour chase with PBS and 0.05% BSA. Supernatants were collected; neutral fats extracted and separated using TLC. TG spots were scraped and counted and results normalized to protein concentration. Data are expressed as mean ± SEM for triplicate wells of 2 independent experiments. (**B**) Densitometric analysis of untransfected, mock and siIQGAP2 transfected HepG2 cells. Single asterisk indicates $p<0.05$. Double asterisk indicates $p<0.005$

results on control diets, *mIqgap2*$^{-/-}$ mice fed high fat were ~50% fatter than wild type, and gained 25% more weight (**Figure 16A**). Furthermore, Oil Red O staining of liver sections reveals little fatty inclusion in *mIqgap2*$^{-/-}$ mice whereas wild type livers are grossly steatotic (**Figure 16B**). Quantification of whole tissue TG content recapitulates the qualitative differences seen in histochemical sections (**Figure 16C**). There was a 2-fold increase in tissue TG content under high fat diet conditions; moreover, comparison of control diet to high fat in *mIqgap2*$^{-/-}$ mice reveals little change in hepatic fatty inclusion. This marked difference between wild type and *mIqgap2*$^{-/-}$ mice reinforces the *ex vivo* and *in vitro* data, implying the defect in TG metabolism impacts fundamental processes in energy utilization.

Altered fuel utilization with high fat diet enhances *mIqgap2*$^{-/-}$ activity.

Analysis of diet-modified mice using indirect calorimetry recapitulates the altered metabolic state of *mIqgap2*$^{-/-}$ mice. While control diet conditions mimic the basal levels initially studied, introduction of high fat yields predictably low RER levels between wild type and *mIqgap2*$^{-/-}$ mice (**Figure 17A**). More interestingly, whereas under control diet conditions, *mIqgap2*$^{-/-}$ mouse activity is attenuated in both the diurnal and nocturnal phases, consumption of high fat elevates the activity levels of *mIqgap2*$^{-/-}$ mice to greater than or indistinguishable amounts as compared to wild type (**Figure 17B**). These data suggests that *mIqgap2*$^{-/-}$ mice generally prefer FA for fuel and that under standard chow conditions do not sense sufficient amounts of FA. Considering their higher

Figure 16

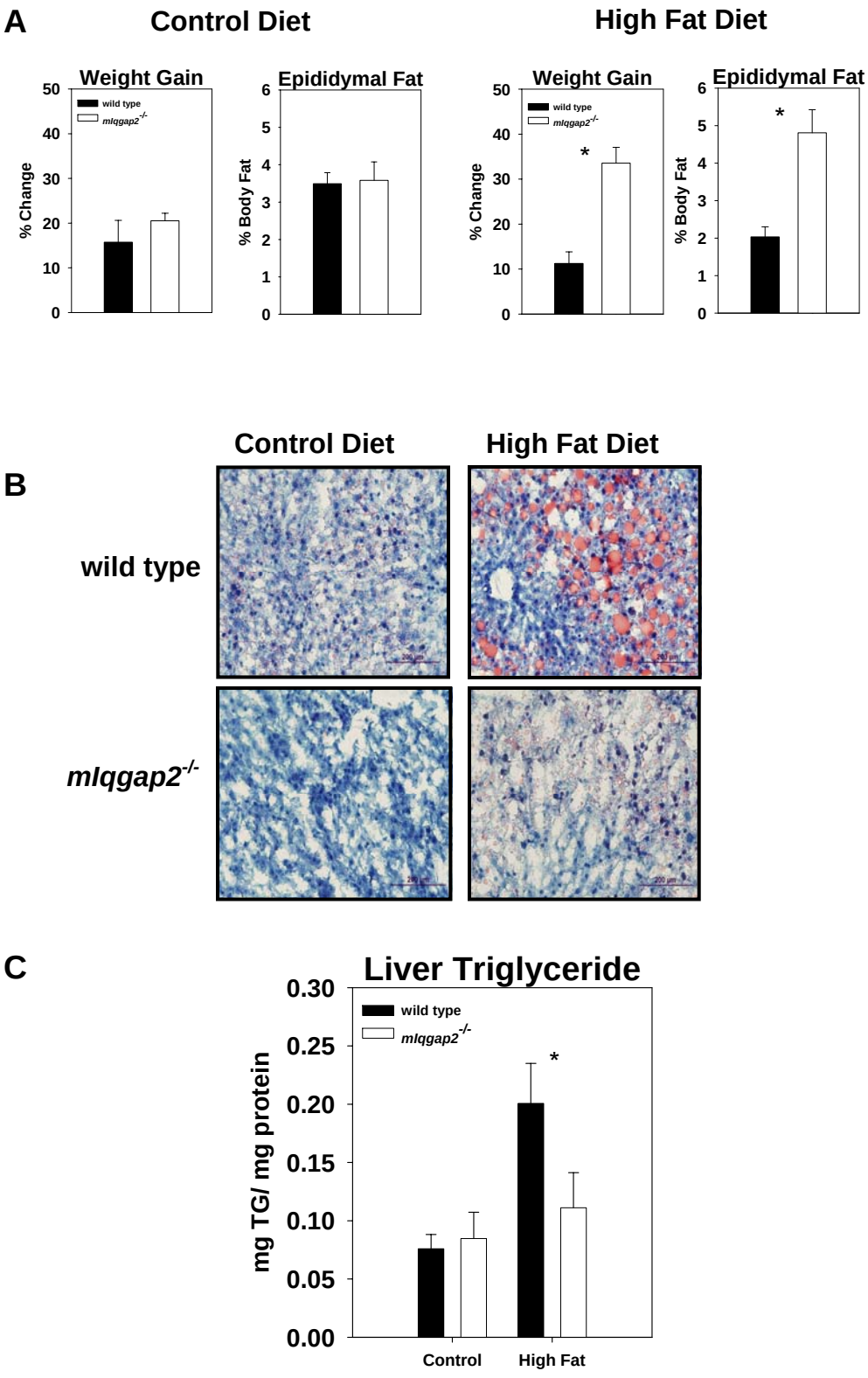
A
Control Diet
High Fat Diet
Weight Gain
Epididymal Fat
% Change
% Body Fat
wild type
mlqgap2-/-
*
B
Control Diet
High Fat Diet
wild type
mlqgap2-/-
C
Liver Triglyceride
mg TG/ mg protein
0.30
0.25
0.20
0.15
0.10
0.05
0.00
Control
High Fat

Figure 16: *mIqgap2*$^{-/-}$ mice do not suffer from steatosis when challenged with high fat. Sixteen-week-old wild type and *mIqgap2*$^{-/-}$ mice were placed on control (10% kcal from fat) or high fat diets (45% kcal) for 6 weeks then assessed for (**A**) weight gain and animal body fat percentage, (**B**) hepatic morphology by Oil Red O staining, and (**C**) hepatic TG quantification. Oil Red O staining was accomplished by submerging isolated liver tissues in cryosectioning medium and freezing overnight at -80^{O}C. Livers were then sectioned and stained for neutral fats by Oil Red O staining with Hematoxylin counterstaining. To quantify hepatic TG content, freshly isolated liver tissues were homogenized in PBS and lipids extracted with chloroform:methanol:sulfuric acid (2:1:0.5%). After washing, the organic phase was dried under nitrogen and resuspended in 2% Triton-X 100. TG were quantified using a serum triglyceride determination assay. Data represented is expressed as mean ± SEM of n=3 mice for body composition and for hepatic TG quantification n=6 for wild type and n=5 for *mIqgap2*$^{-/-}$. Asterisk indicates $p<0.05$

Figure 17

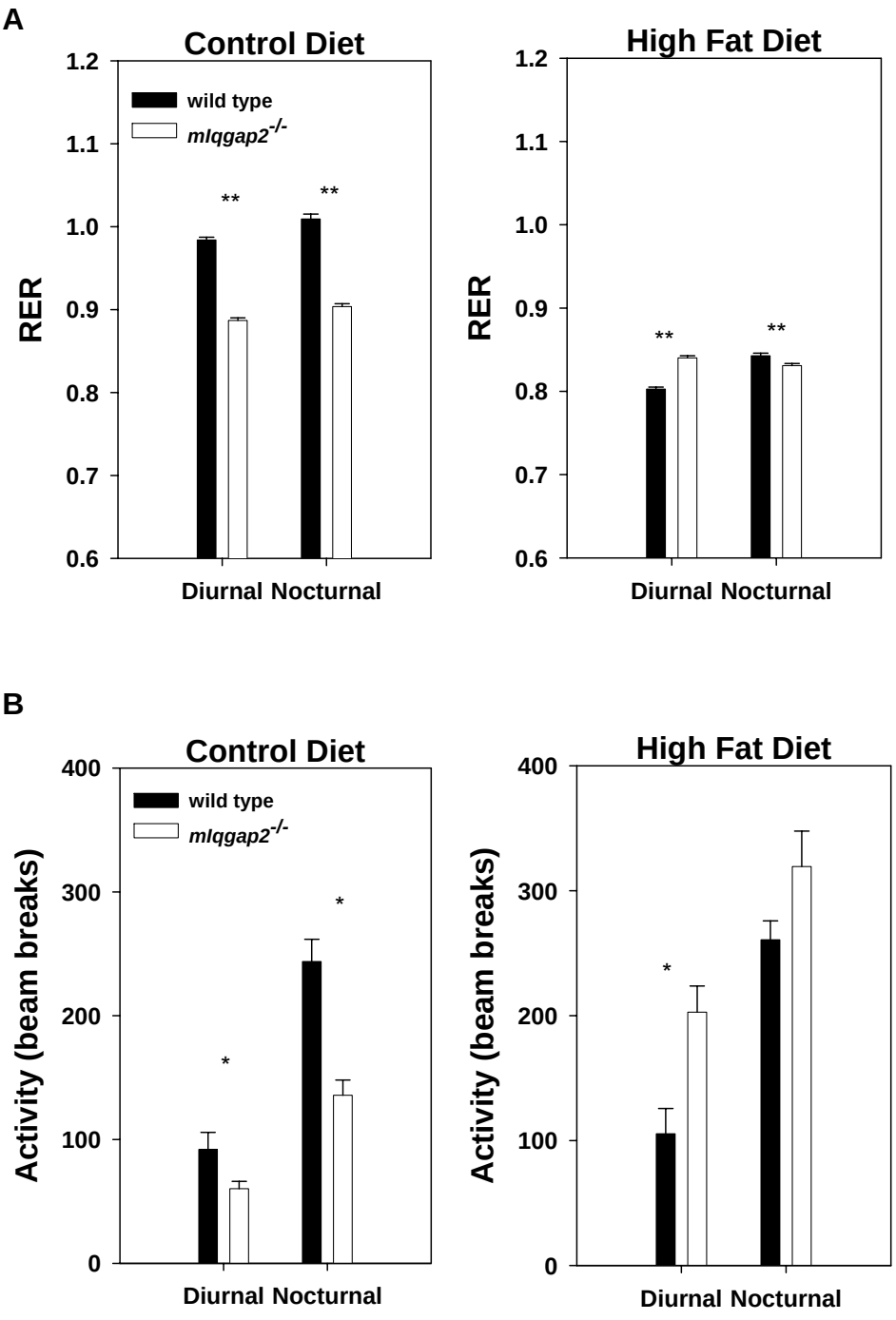
A
Control Diet
High Fat Diet
wild type
mlqgap2-/-
RER
1.2
1.1
1.0
0.9
0.8
0.7
0.6
**
Diurnal Nocturnal
B
Activity (beam breaks)
400
300
200
100
0
*

Figure 17: Altered fuel selection by high fat diet increases *mIqgap2*$^{-/-}$ activity. Prior to completion of the diet study, wild type and *mIqgap2*$^{-/-}$ were subjected to indirect calorimetry to assess VO_2 consumption and VCO_2 release to calculate **(A)** RER and **(B)** direct measurement of activity over 3 day / night cycles. Data is mean of triplicate mice ± SEM for all 3 cycles n=3 for each genotype. Single asterisk indicates $p<0.05$. Double asterisk indicates $p<0.005$.

metabolic rates, this explains the lower activity levels. However, when excessive FA is introduced, sufficient amounts of preferred fuel are present, allowing for normalization of activity levels.

GLUT4 levels in *mIqgap2*$^{-/-}$ muscle is unresponsive to refeeding.

Based on data from indirect calorimetry and the effects seen on the high fat diet, we postulated that muscle is acting as one of the compensatory mechanisms for the increased export of TG from the liver by decreasing glucose utilization. To demonstrate the altered utilization of glucose in muscle, we probed both fasted and postprandial skeletal muscle for GLUT4. Interestingly, under postprandial conditions, there is nearly a 10-fold increase in GLUT4 expression in wild type mice (**Figure 18**) by densitometric analysis. More so, there is little (1.6-fold) increase of GLUT4 expression in fasted versus fed *mIqgap2*$^{-/-}$ GLUT4. Furthermore, glucose tolerance tests (GTT) in *mIqgap2*$^{-/-}$ mice display a diminished rate of glucose clearance as compared to wild type controls (**Figure 19A**). Analysis of wild type insulin levels reveals a predictable response to glucose whereas *mIqgap2*$^{-/-}$ mice maintain high levels of insulin throughout the 2 hour phase of testing (**Figure 19B**). The impaired rates of glucose clearance seen in the GTT reinforces the diminished levels of GLUT4 seen in postprandial *mIqgap2*$^{-/-}$ mice as well as the decreased RER from indirect calorimetry, implying that muscle tissues could be compensating for the increased output of TG seen *in vitro*.

Figure 18

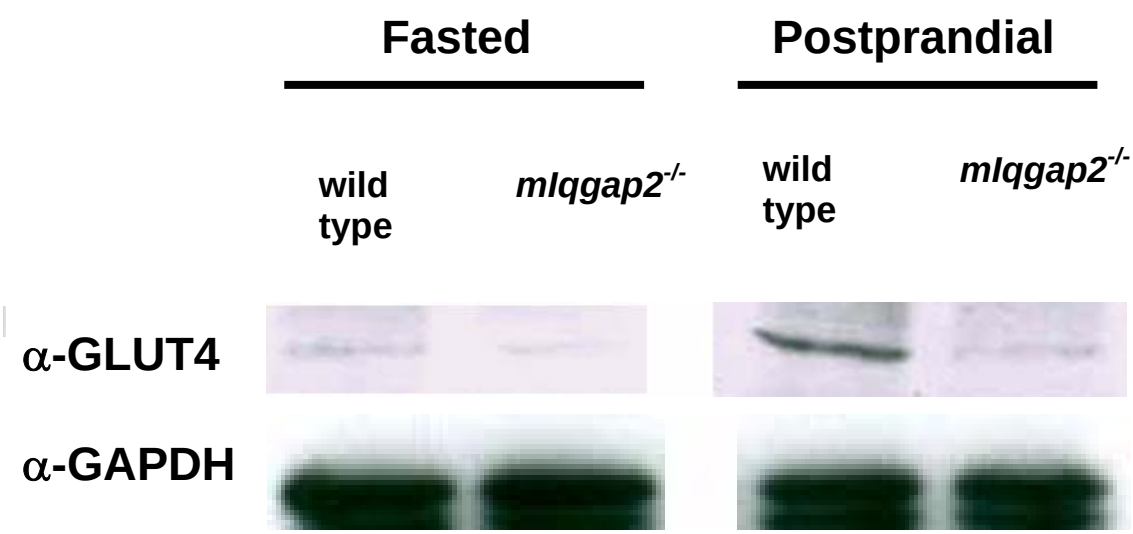
Fasted
Postprandial
wild type
mIqgap2-/-
wild type
mIqgap2-/-
α-GLUT4
α-GAPDH

Figure 18: *mIqgap2*$^{-/-}$ muscle GLUT4 is unresponsive to feeding. Sixteen week old wild type and *mIqgap2*$^{-/-}$ mice were fasted overnight or fasted and then refed for 6 hours to assess muscular GLUT4 response. Mice were sacrificed under anesthesia and gastrocnemius muscle isolated. Muscle was homogenized in lysis buffer and 15 μg total protein was fractionated using SDS-PAGE. After protein transfer to nitrocellulose, membranes were probed for GLUT4 and GAPDH.

Figure 19

A

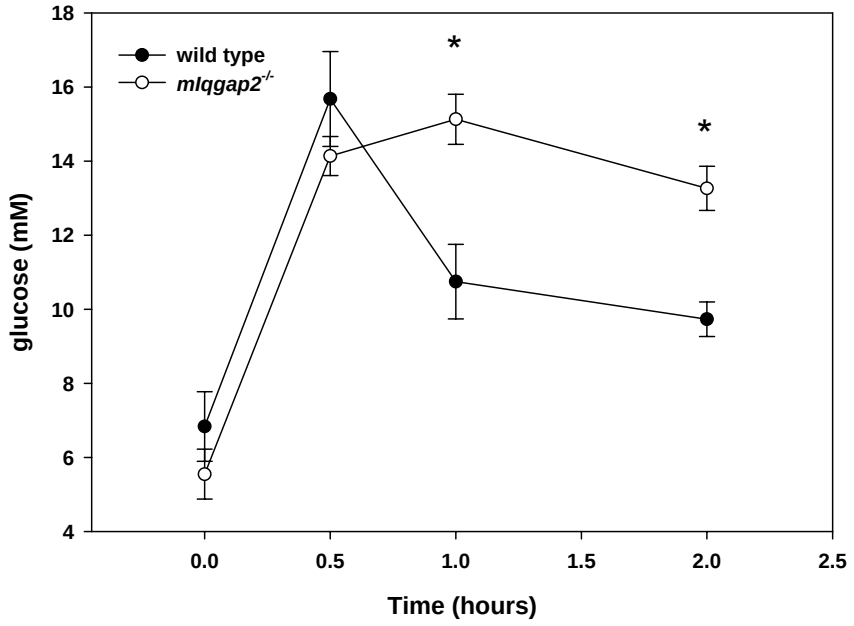
wild type
mlqgap2-/-
glucose (mM)
Time (hours)
*
*
18
16
14
12
10
8
6
4
0.0
0.5
1.0
1.5
2.0
2.5

B

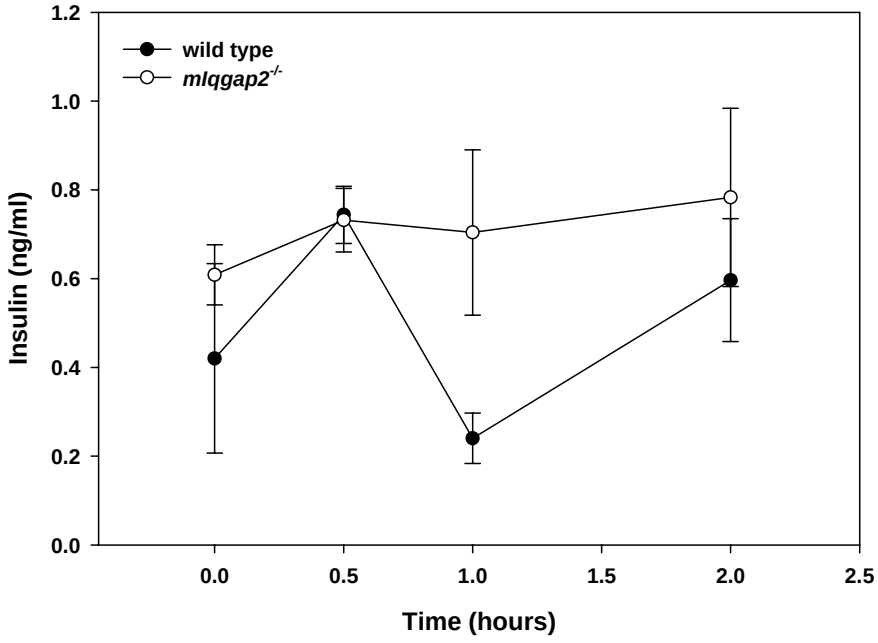
wild type
mlqgap2-/-
Insulin (ng/ml)
Time (hours)
1.2
1.0
0.8
0.6
0.4
0.2
0.0
0.0
0.5
1.0
1.5
2.0
2.5

Figure 19: *mIqgap2*$^{-/-}$ mice display impaired glucose clearance. Sixteen-week-old wild type and *mIqgap2*$^{-/-}$ mice were fasted overnight and intraperitoneally injected with [1,2-$^{13}C_2$]Glucose 1mg / g body weight. Blood samples were obtained by retro-orbital bleeding at t=0, 0.5, 1, and 2 hours to quantify blood glucose (**A**) and (**B**) insulin levels. Data are expressed as mean ± SEM for triplicate mice per genotype. Data and methodology provided by Jun Xu.

Conclusions

Preneoplastic analysis of mIqgap2$^{-/-}$ *mice and metabolism*

In parallel to the HCC phenotype, this work also establishes a novel, physiologically relevant function for IQGAP2 in altering hepatic TG partitioning, with implications for FA regulation in peripheral tissues. Evidence in support of this conclusion is elucidated in both basal indirect calorimetry studies coupled with *ex vivo* and *in vitro* FA utilization studies. The correlative results from *in vivo* diet modification studies provide multiple parallel lines of evidence to the altered metabolism of FA in *mIqgap2*$^{-/-}$ mice.

Analysis of food consumption and body weight reveals an age-dependent decrease in food consumption per unit of body weight, paralleled with data from indirect calorimetry suggests *mIqgap2*$^{-/-}$ mice are metabolically more active in an age-dependent manner. Moreover, it suggests that *mIqgap2*$^{-/-}$ mice require greater caloric intake at earlier ages to meet similar energy demands as wild type. This observation of increased caloric intake with implication of progression to cancer has been observed in prior studies. A wide body of evidence in both human and rodent models suggests that diet restriction increases longevity and significantly reduces the possibility of malignant formation(15, 51). Rats placed on diet restriction and chemically induced to progress to HCC display a diminished rate of HCC onset as compared to non-calorically restricted rats(125). Furthermore, CL57BL/6 x C3H F1 mice, strains known for spontaneous hepatoma formation, placed on diet restriction significantly decreased the number of apoptotic and proliferative hepatocytes, correlating with a decrease in

hepatoma formation(65). While the development of HCC in *mIqgap2*$^{-/-}$ is linked to aberrant signaling of β-catenin(112), it would be interesting to delineate the possibility of the observed increased caloric intake and cancer progression in these mice.

These data presented above, coupled with the functional and structural studies of preneoplastic *mIqgap2*$^{-/-}$ mitochondria gave rise to the possibility a parallel defect in hepatic FA processing may be present, the consequences of which are discussed in more detail below.

Metabolic inflexibility and diabetes in mIqgap2$^{-/-}$ *mice.*

The concept of fuel flexibility is a simplistic thought to a complex milieu of both intraorgan and interorgan signaling. It is a necessity for higher organisms to maintain nutritional homeostasis regardless of fuel source(10, 59, 118). The interplay between glycolysis/glycogenesis and lipogenesis/lipolysis at the interorgan level is tightly regulated by hormones such as insulin, leptin, as well as certain sugar and lipid metabolites(108). Perturbations in these systems due to either certain polygenic traits or environmental conditions such as diet lead to deleterious conditions including obesity, type 2 diabetes, and metabolic syndrome. While numerous phenotypic characterizations of metabolically related proteins exist, this report describes the role of a scaffolding protein as a novel mediator of TG partitioning, with implications as a novel model for the "pre-diabeteic" state. The loss of hepatocyte-specific mIQGAP2 results in redistribution and utilization of TG to muscle and adipose tissue, as defined by the attenuated RER levels and increased body fat composition. This

redistribution is the result of the hypersecretion of TG from hepatocytes as seen in *in vitro* knockdown studies as well as *in vivo* diet modification studies. These data are partly in line with many diabetic disease models. Some of the hallmarks of the diabetic state are hypertriglyceridemia and increased hepatic vLDL secretion(94). Although no molecular interaction has been elucidated to account for the elevated levels of TG secretion, deductive experiments have excluded the possibility for elevated levels of hepatic uptake and oxidation. Moreover, *mIqgap2*$^{-/-}$ mice have a decreased rate of FA uptake within the first 10-12 minutes of FA exposure, indicating the possibility of a defective facilitated transport mechanism. However, *in vitro* experiments using IQGAP2 in cells deficient in FA processing yielded no alteration in FA uptake.

Diet modification of wild type and *mIqgap2*$^{-/-}$ mice exemplifies the altered fuel selection in *mIqgap2*$^{-/-}$ mice. Moderate exposure to high fat dieting results in reduced RER and steatohepatitis in wild type mice to the exclusion of a marked increase in body weight gain or epididymal fat size. Interestingly, *mIqgap2*$^{-/-}$ mice are excluded from steatosis, yet gain 25% more body weight and have nearly 50% more epididymal body fat. Interestingly, mice deficient in liver specific fatty acid binding protein ($FABP_L$) are protected against diet induced steatohepatitis(97). Futhermore, *Fabp1*$^{-/-}$ mice display increased RER levels, suggesting compensatory mechanisms for the defect in hepatic FA uptake(97). Indirect calorimetry suggests that while control diet conditions result in reduced RER and activity in *mIqgap2*$^{-/-}$ mice, introduction of a high fat diet yields more

Figure 20

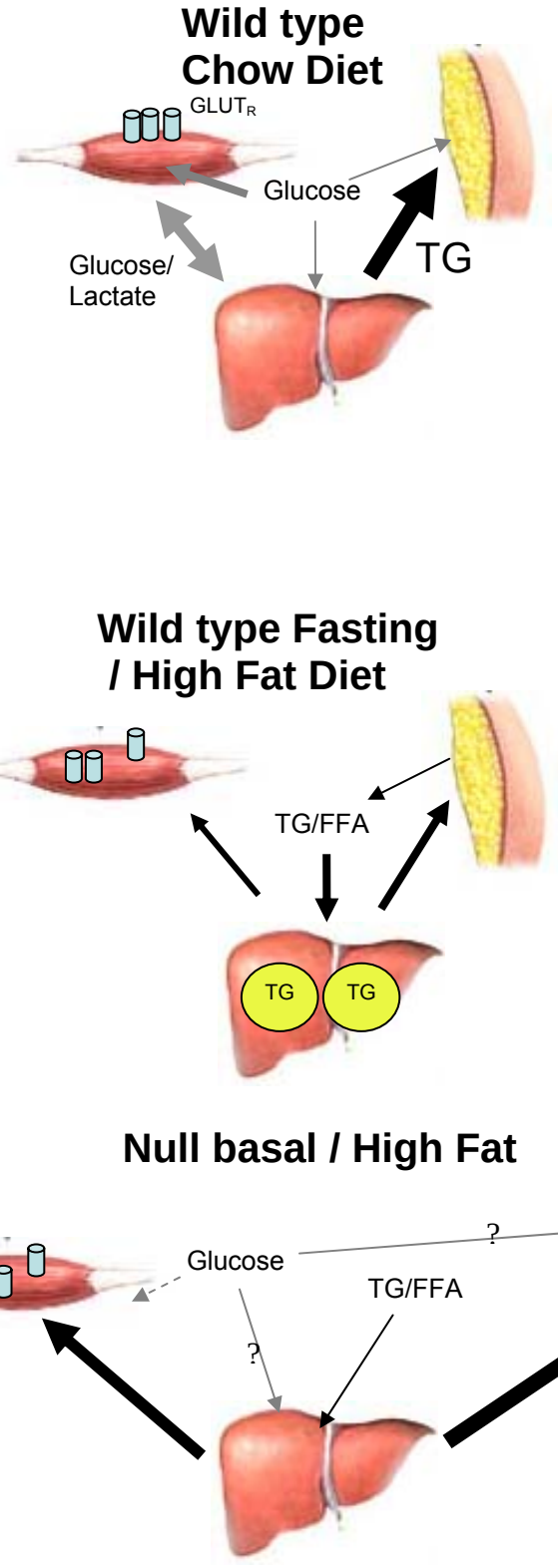
Wild type
Chow Diet
GLUT$_R$
Glucose
Glucose/
Lactate
TG
Wild type Fasting
/ High Fat Diet
TG/FFA
TG
TG
Null basal / High Fat
Glucose
?
TG/FFA
?

Figure 20 Integrated inter-tissue model for altered metabolic fuel switching in *mIqgap2*$^{-/-}$ mice.

Under fasted conditions, wild type mice decrease cell surface GLUT4, and adipose tissue releases TG which are taken up by hepatocytes for FFA processing to deliver to other tissues. Under fed or high fat dieting, GLUT4 is translocated and glucose is taken up for utilization. FFA or TG is taken up by hepatocytes and adipose tissue for storage. *mIqgap2*$^{-/-}$ mice are not as capable of discerning glucose availability, predominantly in muscle where no GLUT4 is present in fed conditions. In fed, fasted or high fat dieting FFA or TG is taken up by the liver then rapidly exported to either adipose tissue for storage or muscle for energy utilization. Grey lines indicate glucose where black indicate TG/FFA. Intensity of lines indicates amount.

useable fuel substrate, as indicated by the increase in activity levels and similarity in RER. This is in accordance with previously reported results in adiponectin receptor 2 null mice (*AdipoR2*$^{-/-}$). *AdipoR2*$^{-/-}$ mice show increased locomotor activity on high fat diet to the exclusion of diet induced obesity(11). These results suggest the possibility that *mIqgap2*$^{-/-}$ mice may not have the capacity to sense glucose as a "primary" fuel in certain tissues and therefore revert to either immediately available serum FA and / or possibly convert large quantities of glucose to FA to provide more preferable substrate (**Figure 20**).

Levels of GLUT4 have been shown to be intimately associated with severity of insulin resistance in both humans and mice(60). To understand the metabolic consequence of increased peripheral FA utilization on glucose metabolism in muscle tissue, preliminary analysis detailing GLUT4 expression was performed. Wild type and *mIqgap2*$^{-/-}$ mice display normal GLUT4 responses to fasting. However, feeding does not result in the increased expression of GLUT4 in *mIqgap2*$^{-/-}$ muscle. The absence of expression of IQGAP2 in muscle(29) suggests that the GLUT4 deficiency is due to either increased insulin resistance or chronic lipid exposure. Indeed, long term exposure to FA has been shown to impair GLUT4 expression(60). Based on basal and refed insulin levels, glucose tolerance testing and the marked reduction in RER in *mIqgap2*$^{-/-}$ mice, it is plausible to conclude that muscle tissue is acting as one compensatory mechanism for the altered TG secretion in hepatocytes. However, more deductive experimentation to understand muscle β-oxidation and hepatic glucose production needs to be performed to more solidify this hypothesis.

Future Directions

The observations detailing IQGAP2 as a novel genetic model for both HCC as well as hepatic TG partitioning allow us to address many standing questions in regards to the IQGAP family of proteins as well as create many new avenues of thought into the molecular actions of IQGAP2. In comparing the pheontypes of the *mIqgap1*$^{-/-}$, *mIqgap2*$^{-/-}$ and *mIqgap1*$^{-/-}$/*mIqgap2*$^{-/-}$ mice, it is clear that the IQGAP family is not functionally redundant, but that IQGAP2 has distinct functions from IQGAP1; furthermore, IQGAP2 acts as a negative regulator of IQGAP1. While the *mIqgap1*$^{-/-}$ mouse has no overt phenotype aside from gastric hyperplasia, the *mIqgap2*$^{-/-}$ mouse is prone to age-dependent development of HCC as well as diabetes-like syndromes. Furthermore, the *mIqgap1*$^{-/-}$/*mIqgap2*$^{-/-}$ mouse is phenotypically normal in regards to HCC progression. This important observation of the double knockout mouse (along with detailed molecular studies) demonstrates the negative regulation of IQGAP2 over IQGAP1. Analysis of *mIqgap1*$^{-/-}$/*mIqgap2*$^{-/-}$ mice in regards to TG partitioning and fuel utilization has yet to be performed. A likely outcome would be similar to the HCC observation in that *mIqgap1*$^{-/-}$/*mIqgap2*$^{-/-}$ mice are indistinguishable from wild type. However, these assumptions are based on uniform expression of IQGAP1 and IQGAP2 in murine tissues.

What would still support the possibility of redundancy are the variations in tissue expression of both IQGAP1 and IQGAP2. Expression of IQGAP1 and IQGAP2 are not stoichiometrically equal in any murine tissue. An interesting genetic experiment would be liver-specific overexpression of IQGAP1 in an

IQGAP2-deficient mouse. Does this mouse develop HCC or diabetes? Based on the notion that IQGAPs are not functionally redundant, one would predict no. Furthermore, *in vitro* co-expression experiments from other labs also point to this conclusion, based on observations that IQGAPs have different baso-apical localization within the same cell, suggesting differing functions.

Under the assumption that IQGAPs are not functionally redundant poses the most relevant question: what, if any, proteins does IQGAP2 interact with that are IQGAP1 does not? I*n vitro* immunoprecipitation experiments after various physiological stimuli (starvation, insulin-stimulated, etc) coupled with mass spectrometry would yield a reasonable mass of data. Furthermore, loss of IQGAP2 yields 2 distinct phenotypes; are they related in any way? These questions are examined in detail below.

IQGAPs and implications in the PI3K / Akt pathway

Our lab has reported the characterization of *mIqgap2*$^{-/-}$ mice as a novel model for HCC(112). While this current report describes these mice as defective in metabolic fuel switching with associated diabetes-like symptoms, the disparate observations made here and in our prior manuscripts may not be entirely unrelated. A wide body of evidence suggests that obesity and diabetes share common pathways with the onset of HCC(38, 39, 66). Our prior report on *mIqgap2*$^{-/-}$-induced HCC is a result of perturbations in the Wnt/β-catenin signaling pathway. However this assessment is based on mortality and tumor specific analysis, revealing loss of membrane bound β-catenin and E-Cadherin with correlative increases in cyclin D1. Analysis of the Insulin Receptor / PI3K / Akt

pathway in preneoplastic livers may prove worthwhile (**Figure 21**) to further understand the molecular basis for the onset of HCC. More specifically, a more thorough understanding of the activity of Glycogen Synthase Kinase 3β (GSK-3β) and Akt in both the carcinomic and prediabetic *mIqgap2*$^{-/-}$ mouse is needed; each of which is discussed in some detail below.

The receptor activated PI3K pathway, like many other signal transduction pathways, is implicated in numerous cellular processes and is stimulated by extracellular ligands to tranduce intracellular processes(100). Furthermore, perturbations in certain PI3K effectors result in loss of downstream signaling which do lead to diseases such as cancer and diabetes(46, 62). PI3K, a heterodimer comprised of one regulatory and one kinase domain, is directly responsible for the phosphorylation of PIP_2 to form active PIP_3, which, in turn, recruits Akt to the cell membrane for "primed" activation by PDK1 on threonine-308(100). PI3K can also directly activate Rac(74), a GTPase modulated by IQGAP1. Additionally PI3K is also activated by E-Cadherin, implicating PI3K in certain cell adhesive pathways(103). Upregulation of PI3K, specifically overexpression of *PIK3CA* (p110α catalytic subunit gene), has been discovered in certain ovarian and cervical tumors, conferring PI3K as a pro-oncogene(85, 115).

Negative regulation of PI3K occurs via dephosphorylation of PIP_3 via PTEN(100). Loss of PTEN through somatic or germline mutations has been associated with various brain, ovary, and prostate cancers, giving rise to the

Figure 21

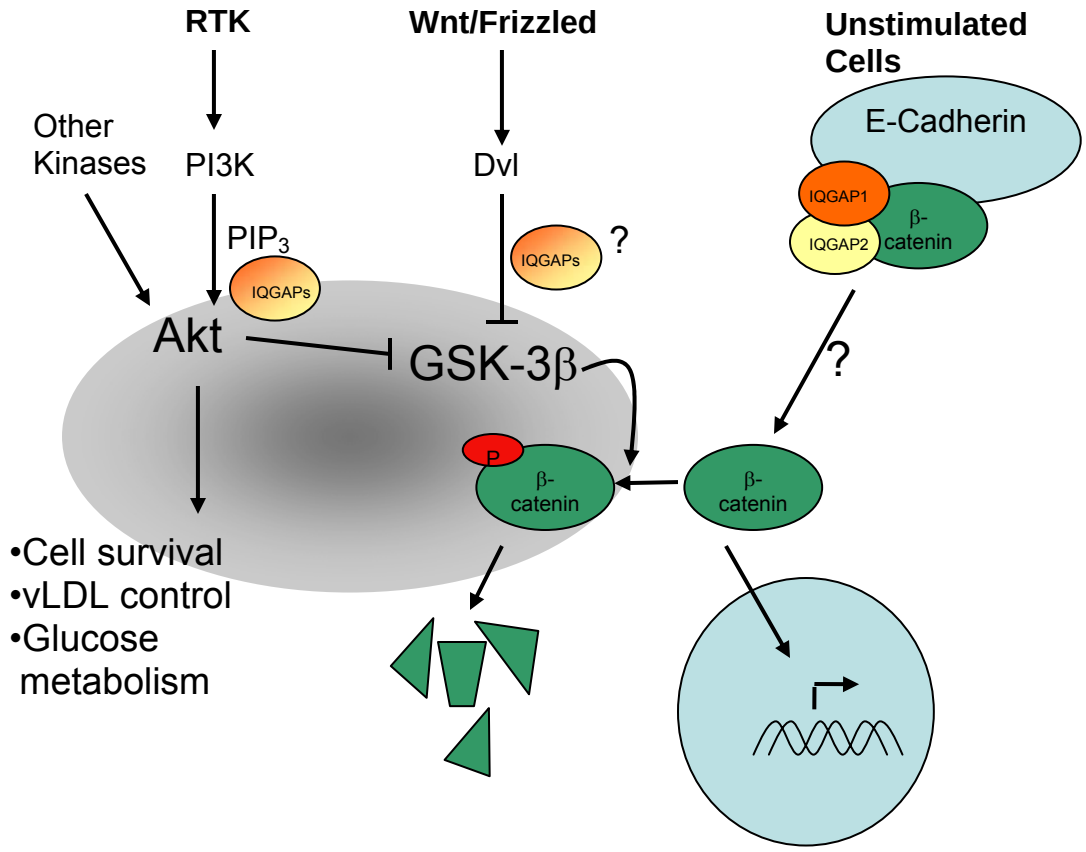
RTK
Wnt/Frizzled
Unstimulated Cells
Other Kinases
PI3K
Dvl
E-Cadherin
IQGAP1
IQGAP2
β-catenin
PIP3
IQGAPs
?
Akt
GSK-3β
?
P
β-catenin
β-catenin
•Cell survival
•vLDL control
•Glucose metabolism

Figure 21: Crosstalk between the Wnt/Frizzled pathway with the PI3K pathway involve Akt and GSK-3β. A description of the commonalities between the Wnt/frizzled / E-Cadherin and PI3K pathways and the possible role IQGAP2 has to account for the phenotypes of hepatocellular carcinoma and diabetes-like observations. IQGAP2 stabilizes IQGAP1 activity at cadherin based cell-cell junctions, and loss of IQGAP2 results in age-dependent hepatocellular carcinoma, through the activation of β-catenin, which is normally degraded at basal conditions. The regulation of Akt at the cell membrane by IQGAP2 and / or IQGAP1 provides a plausible means to define how IQGAP2 may regulate both hepatic TG secretion as well as β-catenin regulation through GSK-3β. Loss of IQGAP2 would deregulate Akt activation, resulting in increased levels of TG secretion. The shaded area denotes a common node of signaling between the 2 pathways.

possibility that PTEN acts as a tumor suppressor(14). Furthermore, hepatocyte-specific PTEN deleted mice (*AlbCrePten*$^{flox/flox}$) are prone to steatohepatitis and HCC(62), implicating PTEN in fundamental processes of hepatocyte stability and metabolism.

Akt (Protein Kinase B, PKB) is the major downstream effector of PI3K and serves as an intermediate kinase for phosphorylation of various effectors of cellular processes(46). In humans and mice, three isoforms (Akt1 (PKBα), Akt2 (PKBβ) and Akt3 (PKBγ)) exist, all derived from distinct genes located on chromosomes 14q32, 19q13, and 1q43, respectively(100). While all three isoforms are activated by similar mechanisms and affect similar downstream proteins, the distinction between the three lies loosely in tissue distribution. Akt1 & 2 are broadly expressed whereas Akt3 is restricted to brain and testis(100). After the "primed" activation by PI3K, full activation of Akt occurs via phosphorylation of a second site, serine-473(100). Activators responsible for its phosphorylation are not fully understood, although kinases such as PDK1 have been described(5). Akt also has pro-oncogenic capabilities, either through upregulation of PI3K(104), downregulation of PTEN(14), or direct upregulation of Akt(137). Interestingly, microcystin induced transformation of colorectal cells results in upregulation of Akt. In parallel, the upregulation of numerous GAPs, including IQGAP2, was observed. Whether or not the upregulation of IQGAP2 is directly due to Akt upregulation remains to be discovered. *Akt* knockout mice for two of the three isoforms have been produced. Although the three share similar structure and function, knockouts for *Akt1* and *Akt2* generate distinct phenotypes.

Akt1$^{-/-}$ mice are stunted in growth and have decreased life spans, especially when exposed to genotoxic stress(23). Conversely, *Akt2*$^{-/-}$ animals display predominantly a diabetic phenotype, characterized by decreased peripheral glucose disposal, predominantly due to insulin resistance in muscle and liver tissues(25). Interestingly, in fructose fed diabetic hampsters, an increase in vLDL secretion is correlated with decreased atypical Protein Kinase C (aPKC) and Akt levels(120).

GSK-3β serves as a common point of divergence between the PI3K / Akt and Wnt/Frizzled signaling pathways(35). Initially described for its ability to modulate glycogen synthesis(41), GSK-3β has also been described to effect neuronal generation and body pattern formation(52). Deregulation of GSK-3 proteins is also implicated in numerous diseases including Alzheimer's disease(86), bipolar disorder(33), diabetes(68), and cancer(6). Under basal conditions, GSK-3 proteins are constitutively activated via tyrosine-216 phosphoryation and inhibited by serine-9 phosphorylation through numerous effector kinases such as Akt, disheveled (Dsh), and Cdc42(35).

Collective data from this study and the report detailing the HCC phenotype would suggest a decreased level of phosphorylation of GSK-3β in hepatocytes, primarily due to loss of Akt. *mIqgap2*$^{-/-}$ mice display "pre-diabetic" conditions characterized by impaired glucose clearance and elevated insulin levels to the exclusion of steatosis. Parallel *in vitro* experiments reveal increased levels of TG secretion. While no molecular evidence exists for interactions between IQGAPs and proteins in the PI3K / Akt pathway, previous reports detailing IQGAP1

localization in PIP_2 rich lipid rafts in leading edge motility(56) is suggestive that IQGAP1 and / or IQGAP2 colocalize to these rafts to allow for immediate signal transduction upon PIP_2 phosphorylation to PIP_3 via PI3K in alternate signaling pathways. Therefore, it is reasonable to hypothesize that IQGAP2 directly interacts with Akt (or indirectly through IQGAP1) for cell surface recruitment. The predominant hypothesis would suggest that loss of IQGAP2 limits Akt cell surface recruitment, therefore limited activation via threonine-308 phosphorylation. This would result in the aforementioned hepatic metabolic phenotype, and in parallel would affect GSK-3β by allowing constitutive activation and β-catenin degradation. In conjunction with the known role of IQGAPs in cadherin-catenin complex formation and Wnt signaling, this novel association with Akt may serve as the first hit in the prototypical 2-hit hypothesis in cancer progression.

To better understand the role of IQGAP2 in metabolic regulation, detailed experiments to better understand glucose and lipid formation/utilization are of great importance. How would hyperinsulinemic / euglycemic clamps affect *mIqgap2*$^{-/-}$ peripheral tissues and hypoinsulinemic / euglycemic clamping affect the liver glucose metabolism? How is *de novo* lipogenesis affected? Based on prior data, one would expect a decrease in hepatic lipogenesis and an increase in adipose lipogenesis. How is glucose utilized in peripheral tissues? Detailed GTT experiments with labeled glucose would prove worthwhile. By tracing two different isomers of glucose ([2-H^2]- and [6,6-H^2]-glucose) in a GTT, one can assess the futile recycling of glucose, that is, the wasted recycling of glucose

metabolites (gluocose ↔ glucose-6-phosphate)(134). A greater percentage of [6,6-H^2]-glucose over [2-H^2]-glucose in blood plasma over a given period of time is suggestive of an increase in hepatic futile glucose cycling, and an increased utilization by peripheral tissues. Based on the data presented here, one would predict a decrease in hepatic glucose cycling, and therefore, a decrease in peripheral glucose utilization. Lastly, data from *mIqgap1*$^{-/-}$*/mIqgap2*$^{-/-}$ mice in the progression of HCC demonstrate the regulatory role of IQGAP2 on IQGAP1. Would parallel metabolic experiments in these mice yield results similar to wild type? While the outcomes to these questions remain theoretical, what is certain is how *mIqgap2*$^{-/-}$ mice will certainly contribute to ongoing diabetes and cancer research. More so, they exemplify a necessity to metabolically characterize knockout mice as to further understand the whole animal effects due to either single gene or tissue restricted knockouts.

References

1. **Accili D, Drago J, Lee EJ, Johnson MD, Cool MH, Salvatore P, Asico LD, Jose PA, Taylor SI, and Westphal H.** Early neonatal death in mice homozygous for a null allele of the insulin receptor gene. *Nature genetics* 12: 106-109, 1996.

2. **ADA.** American Diabetes Assoication.

3. **Adams LA, Lymp JF, St Sauver J, Sanderson SO, Lindor KD, Feldstein A, and Angulo P.** The natural history of nonalcoholic fatty liver disease: a population-based cohort study. *Gastroenterology* 129: 113-121, 2005.

4. **Bahou WF, Scudder L, Rubenstein D, and Jesty J.** A shear-restricted pathway of platelet procoagulant activity is regulated by IQGAP1. *J Biol Chem* 279: 22571-22577, 2004.

5. **Balendran A, Casamayor A, Deak M, Paterson A, Gaffney P, Currie R, Downes CP, and Alessi DR.** PDK1 acquires PDK2 activity in the presence of a synthetic peptide derived from the carboxyl terminus of PRK2. *Curr Biol* 9: 393-404, 1999.

6. **Ban KC, Singh H, Krishnan R, and Seow HF.** GSK-3beta phosphorylation and alteration of beta-catenin in hepatocellular carcinoma. *Cancer letters* 199: 201-208, 2003.

7. **Barbin A, Froment O, Boivin S, Marion MJ, Belpoggi F, Maltoni C, and Montesano R.** p53 gene mutation pattern in rat liver tumors induced by vinyl chloride. *Cancer research* 57: 1695-1698, 1997.

8. **Bastie CC, Zong H, Xu J, Busa B, Judex S, Kurland IJ, and Pessin JE.** Integrative Metabolic Regulation of Peripheral Tissue Fatty Acid Oxidation by the Src Kinase Family Member Fyn. *Cell Metabolism* 5: 371-381, 2007.

9. **Bell GI, Horita S, and Karam JH.** A polymorphic locus near the human insulin gene is associated with insulin-dependent diabetes mellitus. *Diabetes* 33: 176-183, 1984.

10. **Bickel PE.** Metabolic fuel selection: the importance of being flexible. *J Clin Invest* 114: 1547-1549, 2004.

11. **Bjursell M, Ahnmark A, Bohlooly YM, William-Olsson L, Rhedin M, Peng XR, Ploj K, Gerdin AK, Arnerup G, Elmgren A, Berg AL, Oscarsson J, and Linden D.** Opposing effects of adiponectin receptors 1 and 2 on energy metabolism. *Diabetes* 56: 583-593, 2007.

12. **Bluher M, Kahn BB, and Kahn CR.** Extended longevity in mice lacking the insulin receptor in adipose tissue. *Science (New York, NY* 299: 572-574, 2003.

13. **Bogenhagen D and Clayton DA.** The number of mitochondrial deoxyribonucleic acid genomes in mouse L and human HeLa cells. Quantitative isolation of mitochondrial deoxyribonucleic acid. *J Biol Chem* 249: 7991-7995, 1974.

14. **Bonneau D and Longy M.** Mutations of the human PTEN gene. *Human mutation* 16: 109-122, 2000.

15. **Bordone L and Guarente L.** Calorie restriction, SIRT1 and metabolism: understanding longevity. *Nature reviews* 6: 298-305, 2005.

16. **Bressac B, Kew M, Wands J, and Ozturk M.** Selective G to T mutations of p53 gene in hepatocellular carcinoma from southern Africa. *Nature* 350: 429-431, 1991.

17. **Briggs MW, Li Z, and Sacks DB.** IQGAP1-mediated stimulation of transcriptional co-activation by beta-catenin is modulated by calmodulin. *J Biol Chem* 277: 7453-7465, 2002.

18. **Briggs MW and Sacks DB.** IQGAP1 as signal integrator: Ca2+, calmodulin, Cdc42 and the cytoskeleton. *FEBS Lett* 542: 7-11, 2003.

19. **Brill S, Li S, Lyman CW, Church DM, Wasmuth JJ, Weissbach L, Bernards A, and Snijders AJ.** The Ras GTPase-activating-protein-related human protein IQGAP2 harbors a potential actin binding domain and interacts with calmodulin and Rho family GTPases. *Molecular and cellular biology* 16: 4869-4878, 1996.

20. **Brown AJ, Jupe S, and Briscoe CP.** A family of fatty acid binding receptors. *DNA and cell biology* 24: 54-61, 2005.

21. **Bruning JC, Michael MD, Winnay JN, Hayashi T, Horsch D, Accili D, Goodyear LJ, and Kahn CR.** A muscle-specific insulin receptor knockout exhibits features of the metabolic syndrome of NIDDM without altering glucose tolerance. *Molecular cell* 2: 559-569, 1998.

22. **Bucolo G and David H.** Quantitative determination of serum triglycerides by the use of enzymes. *Clinical chemistry* 19: 476-482, 1973.

23. **Chen WS, Xu PZ, Gottlob K, Chen ML, Sokol K, Shiyanova T, Roninson I, Weng W, Suzuki R, Tobe K, Kadowaki T, and Hay N.** Growth retardation and increased apoptosis in mice with homozygous disruption of the Akt1 gene. *Genes & development* 15: 2203-2208, 2001.

24. **Chmurzynska A.** The multigene family of fatty acid-binding proteins (FABPs): function, structure and polymorphism. *Journal of applied genetics* 47: 39-48, 2006.

25. **Cho H, Mu J, Kim JK, Thorvaldsen JL, Chu Q, Crenshaw EB, 3rd, Kaestner KH, Bartolomei MS, Shulman GI, and Birnbaum MJ.** Insulin resistance and a diabetes mellitus-like syndrome in mice lacking the protein kinase Akt2 (PKB beta). *Science (New York, NY* 292: 1728-1731, 2001.

26. **Colnot S, Decaens T, Niwa-Kawakita M, Godard C, Hamard G, Kahn A, Giovannini M, and Perret C.** Liver-targeted disruption of Apc in mice activates beta-catenin signaling and leads to hepatocellular carcinomas. *Proceedings of the National Academy of Sciences of the United States of America* 101: 17216-17221, 2004.

27. **Csukly K, Ascah A, Matas J, Gardiner PF, Fontaine E, and Burelle Y.** Muscle denervation promotes opening of the permeability transition pore and increases the expression of cyclophilin D. *The Journal of physiology* 574: 319-327, 2006.

28. **Cunningham CC and Van Horn CG.** Energy availability and alcohol-related liver pathology. *Alcohol Res Health* 27: 291-299, 2003.

29. **Cupit LD, Schmidt VA, Miller F, and Bahou WF.** Distinct PAR/IQGAP expression patterns during murine development: implications for thrombin-associated cytoskeletal reorganization. *Mamm Genome* 15: 618-629, 2004.

30. **Davies JL, Kawaguchi Y, Bennett ST, Copeman JB, Cordell HJ, Pritchard LE, Reed PW, Gough SC, Jenkins SC, Palmer SM, and et al.** A genome-wide search for human type 1 diabetes susceptibility genes. *Nature* 371: 130-136, 1994.

31. **de La Coste A, Romagnolo B, Billuart P, Renard CA, Buendia MA, Soubrane O, Fabre M, Chelly J, Beldjord C, Kahn A, and Perret C.** Somatic mutations of the beta-catenin gene are frequent in mouse and human hepatocellular carcinomas. *Proceedings of the National Academy of Sciences of the United States of America* 95: 8847-8851, 1998.

32. **De Vivo I, Marion MJ, Smith SJ, Carney WP, and Brandt-Rauf PW.** Mutant c-Ki-ras p21 protein in chemical carcinogenesis in humans exposed to vinyl chloride. *Cancer Causes Control* 5: 273-278, 1994.

33. **Detera-Wadleigh SD.** Lithium-related genetics of bipolar disorder. *Annals of medicine* 33: 272-285, 2001.

34. **DiabetesMD.** Diabetes Symptoms - Tests and Diagnosis, 2007.

35. **Doble BW and Woodgett JR.** GSK-3: tricks of the trade for a multi-tasking kinase. *Journal of cell science* 116: 1175-1186, 2003.

36. **Doege H, Baillie RA, Ortegon AM, Tsang B, Wu Q, Punreddy S, Hirsch D, Watson N, Gimeno RE, and Stahl A.** Targeted deletion of FATP5 reveals multiple functions in liver metabolism: alterations in hepatic lipid homeostasis. *Gastroenterology* 130: 1245-1258, 2006.

37. **Doege H and Stahl A.** Protein-mediated fatty acid uptake: novel insights from in vivo models. *Physiology (Bethesda, Md* 21: 259-268, 2006.

38. **El-Serag HB and Rudolph KL.** Hepatocellular carcinoma: epidemiology and molecular carcinogenesis. *Gastroenterology* 132: 2557-2576, 2007.

39. **El-Serag HB, Tran T, and Everhart JE.** Diabetes increases the risk of chronic liver disease and hepatocellular carcinoma. *Gastroenterology* 126: 460-468, 2004.

40. **Elmadhoun BM, Wang GQ, Kirshenbaum LA, and Burczynski FJ.** Palmitate uptake by neonatal rat myocytes and hepatocytes. Role of extracellular protein. *European journal of biochemistry / FEBS* 268: 3145-3153, 2001.

41. **Embi N, Rylatt DB, and Cohen P.** Glycogen synthase kinase-3 from rabbit skeletal muscle. Separation from cyclic-AMP-dependent protein kinase and phosphorylase kinase. *European journal of biochemistry / FEBS* 107: 519-527, 1980.

42. **Epp JA and Chant J.** An IQGAP-related protein controls actin-ring formation and cytokinesis in yeast. *Curr Biol* 7: 921-929, 1997.

43. **Fabregat I, Roncero C, and Fernandez M.** Survival and apoptosis: a dysregulated balance in liver cancer. *Liver Int* 27: 155-162, 2007.

44. **Faix J, Weber I, Mintert U, Kohler J, Lottspeich F, and Marriott G.** Recruitment of cortexillin into the cleavage furrow is controlled by Rac1 and IQGAP-related proteins. *The EMBO journal* 20: 3705-3715, 2001.

45. **Farazi PA and DePinho RA.** Hepatocellular carcinoma pathogenesis: from genes to environment. *Nat Rev Cancer* 6: 674-687, 2006.

46. **Farese RV, Sajan MP, and Standaert ML.** Insulin-sensitive protein kinases (atypical protein kinase C and protein kinase B/Akt): actions and defects in obesity and type II diabetes. *Experimental biology and medicine (Maywood, NJ* 230: 593-605, 2005.

47. **Farese RV, Sajan MP, Yang H, Li P, Mastorides S, Gower WR, Nimal S, Choi CS, Kim S, Shulman GI, Kahn CR, Braun U, and Leitges M.** Muscle-specific knockout of PKC-lambda impairs glucose transport and induces metabolic and diabetic syndromes. *J Clin Invest* 117: 2289-2301, 2007.

48. **Fernandez AM, Kim JK, Yakar S, Dupont J, Hernandez-Sanchez C, Castle AL, Filmore J, Shulman GI, and Le Roith D.** Functional inactivation of the IGF-I and insulin receptors in skeletal muscle causes type 2 diabetes. *Genes & development* 15: 1926-1934, 2001.

49. **Fisher RM and Gertow K.** Fatty acid transport proteins and insulin resistance. *Current opinion in lipidology* 16: 173-178, 2005.

50. **Folch J, Lees M, and Sloane Stanley GH.** A simple method for the isolation and purification of total lipides from animal tissues. *J Biol Chem* 226: 497-509, 1957.

51. **Fontana L.** Excessive adiposity, calorie restriction, and aging. *Jama* 295: 1577-1578, 2006.

52. **Frame S and Cohen P.** GSK3 takes centre stage more than 20 years after its discovery. *The Biochemical journal* 359: 1-16, 2001.

53. **Fukata M, Kuroda S, Fujii K, Nakamura T, Shoji I, Matsuura Y, Okawa K, Iwamatsu A, Kikuchi A, and Kaibuchi K.** Regulation of cross-linking of actin filament by IQGAP1, a target for Cdc42. *J Biol Chem* 272: 29579-29583, 1997.

54. **Fukata M, Watanabe T, Noritake J, Nakagawa M, Yamaga M, Kuroda S, Matsuura Y, Iwamatsu A, Perez F, and Kaibuchi K.** Rac1 and Cdc42 Capture Microtubules through IQGAP1 and CLIP-170. *Cell* 109: 873-885, 2002.

55. **Fukuda H and Iritani N.** Regulation of ATP citrate-lyase gene expression in hepatocytes and adipocytes in normal and genetically obese rats. *Journal of biochemistry* 126: 437-444, 1999.

56. **Golub T and Caroni P.** PI(4,5)P2-dependent microdomain assemblies capture microtubules to promote and control leading edge motility. *The Journal of cell biology* 169: 151-165, 2005.

57. **Greenberg CC, Jurczak MJ, Danos AM, and Brady MJ.** Glycogen branches out: new perspectives on the role of glycogen metabolism in the integration of metabolic pathways. *Am J Physiol Endocrinol Metab* 291: E1-8, 2006.

58. **Gundersen GG.** Microtubule capture: IQGAP and CLIP-170 expand the repertoire. *Curr Biol* 12: R645-647, 2002.

59. **Herman MA and Kahn BB.** Glucose transport and sensing in the maintenance of glucose homeostasis and metabolic harmony. *J Clin Invest* 116: 1767-1775, 2006.

60. **Hirabara SM, Silveira LR, Abdulkader F, Carvalho CR, Procopio J, and Curi R.** Time-dependent effects of fatty acids on skeletal muscle metabolism. *Journal of cellular physiology* 210: 7-15, 2007.

61. **Ho YD, Joyal JL, Li Z, and Sacks DB.** IQGAP1 integrates Ca2+/calmodulin and Cdc42 signaling. *J Biol Chem* 274: 464-470, 1999.

62. **Horie Y, Suzuki A, Kataoka E, Sasaki T, Hamada K, Sasaki J, Mizuno K, Hasegawa G, Kishimoto H, Iizuka M, Naito M, Enomoto K, Watanabe S, Mak TW, and Nakano T.** Hepatocyte-specific Pten deficiency results in steatohepatitis and hepatocellular carcinomas. *J Clin Invest* 113: 1774-1783, 2004.

63. **Hu TH, Huang CC, Lin PR, Chang HW, Ger LP, Lin YW, Changchien CS, Lee CM, and Tai MH.** Expression and prognostic role of tumor suppressor gene PTEN/MMAC1/TEP1 in hepatocellular carcinoma. *Cancer* 97: 1929-1940, 2003.

64. **Izumi G, Sakisaka T, Baba T, Tanaka S, Morimoto K, and Takai Y.** Endocytosis of E-cadherin regulated by Rac and Cdc42 small G proteins through IQGAP1 and actin filaments. *The Journal of cell biology* 166: 237-248, 2004.

65. **James SJ and Muskhelishvili L.** Rates of apoptosis and proliferation vary with caloric intake and may influence incidence of spontaneous hepatoma in C57BL/6 x C3H F1 mice. *Cancer research* 54: 5508-5510, 1994.

66. **Jiang JT, Xu N, Zhang XY, and Wu CP.** Lipids changes in liver cancer. *Journal of Zhejiang University Science* 8: 398-409, 2007.

67. **Joyal JL, Annan RS, Ho YD, Huddleston ME, Carr SA, Hart MJ, and Sacks DB.** Calmodulin modulates the interaction between IQGAP1 and Cdc42. Identification of IQGAP1 by nanoelectrospray tandem mass spectrometry. *J Biol Chem* 272: 15419-15425, 1997.

68. **Kaidanovich O and Eldar-Finkelman H.** The role of glycogen synthase kinase-3 in insulin resistance and type 2 diabetes. *Expert opinion on therapeutic targets* 6: 555-561, 2002.

69. **Kerner J and Hoppel C.** Fatty acid import into mitochondria. *Biochimica et biophysica acta* 1486: 1-17, 2000.

70. **Kersten S.** Mechanisms of nutritional and hormonal regulation of lipogenesis. *EMBO Rep* 2: 282-286, 2001.

71. **Kielhorn J, Melber C, Wahnschaffe U, Aitio A, and Mangelsdorf I.** Vinyl chloride: still a cause for concern. *Environmental health perspectives* 108: 579-588, 2000.

72. **Kim MS and Polychronakos C.** Immunogenetics of type 1 diabetes. *Hormone research* 64: 180-188, 2005.

73. **Kim SH, Goto M, and Akaike T.** Specific binding of glucose-derivatized polymers to the asialoglycoprotein receptor of mouse primary hepatocytes. *J Biol Chem* 276: 35312-35319, 2001.

74. **Kotani K, Hara K, Kotani K, Yonezawa K, and Kasuga M.** Phosphoinositide 3-kinase as an upstream regulator of the small GTP-binding protein Rac in the insulin signaling of membrane ruffling. *Biochemical and biophysical research communications* 208: 985-990, 1995.

75. **Kotani K, Peroni OD, Minokoshi Y, Boss O, and Kahn BB.** GLUT4 glucose transporter deficiency increases hepatic lipid production and peripheral lipid utilization. *J Clin Invest* 114: 1666-1675, 2004.

76. **Kuroda S, Fukata M, Kobayashi K, Nakafuku M, Nomura N, Iwamatsu A, and Kaibuchi K.** Identification of IQGAP as a putative target for the small GTPases, Cdc42 and Rac1. *J Biol Chem* 271: 23363-23367, 1996.

77. **Lavanchy D.** Hepatitis B virus epidemiology, disease burden, treatment, and current and emerging prevention and control measures. *Journal of viral hepatitis* 11: 97-107, 2004.

78. **LeRoith D and Gavrilova O.** Mouse models created to study the pathophysiology of Type 2 diabetes. *The international journal of biochemistry & cell biology* 38: 904-912, 2006.

79. **Leung MC, Diaz-Llano G, and Smith TK.** Mycotoxins in pet food: a review on worldwide prevalence and preventative strategies. *Journal of agricultural and food chemistry* 54: 9623-9635, 2006.

80. **Li Q and Stuenkel EL.** Calcium negatively modulates calmodulin interaction with IQGAP1. *Biochemical and biophysical research communications* 317: 787-795, 2004.

81. **Li S, Wang Q, Chakladar A, Bronson RT, and Bernards A.** Gastric hyperplasia in mice lacking the putative Cdc42 effector IQGAP1. *Molecular and cellular biology* 20: 697-701, 2000.

82. **Li Z, Kim SH, Higgins JM, Brenner MB, and Sacks DB.** IQGAP1 and calmodulin modulate E-cadherin function. *J Biol Chem* 274: 37885-37892, 1999.

83. **Liao J, Sportsman R, Harris J, and Stahl A.** Real-time quantification of fatty acid uptake using a novel fluorescence assay. *Journal of lipid research* 46: 597-602, 2005.

84. **Lippincott J and Li R.** Sequential assembly of myosin II, an IQGAP-like protein, and filamentous actin to a ring structure involved in budding yeast cytokinesis. *The Journal of cell biology* 140: 355-366, 1998.

85. **Ma YY, Wei SJ, Lin YC, Lung JC, Chang TC, Whang-Peng J, Liu JM, Yang DM, Yang WK, and Shen CY.** PIK3CA as an oncogene in cervical cancer. *Oncogene* 19: 2739-2744, 2000.

86. **Maccioni RB, Munoz JP, and Barbeito L.** The molecular bases of Alzheimer's disease and other neurodegenerative disorders. *Archives of medical research* 32: 367-381, 2001.

87. **Macias MJ, Wiesner S, and Sudol M.** WW and SH3 domains, two different scaffolds to recognize proline-rich ligands. *FEBS Lett* 513: 30-37, 2002.

88. **Mateer SC, Morris LE, Cromer DA, Bensenor LB, and Bloom GS.** Actin filament binding by a monomeric IQGAP1 fragment with a single calponin homology domain. *Cell motility and the cytoskeleton* 58: 231-241, 2004.

89. **Mateer SC, Wang N, and Bloom GS.** IQGAPs: integrators of the cytoskeleton, cell adhesion machinery, and signaling networks. *Cell motility and the cytoskeleton* 55: 147-155, 2003.

90. **Mattiazzi A, Vittone L, and Mundina-Weilenmann C.** Ca2+/calmodulin-dependent protein kinase: a key component in the contractile recovery from acidosis. *Cardiovascular research* 73: 648-656, 2007.

91. **McCallum SJ, Wu WJ, and Cerione RA.** Identification of a putative effector for Cdc42Hs with high sequence similarity to the RasGAP-related protein IQGAP1 and a Cdc42Hs binding partner with similarity to IQGAP2. *J Biol Chem* 271: 21732-21737, 1996.

92. **McGlynn KA, Rosvold EA, Lustbader ED, Hu Y, Clapper ML, Zhou T, Wild CP, Xia XL, Baffoe-Bonnie A, Ofori-Adjei D, and et al.** Susceptibility to hepatocellular carcinoma is associated with genetic variation in the enzymatic detoxification of aflatoxin B1. *Proceedings of the National Academy of Sciences of the United States of America* 92: 2384-2387, 1995.

93. **Melen K, Fagerlund R, Nyqvist M, Keskinen P, and Julkunen I.** Expression of hepatitis C virus core protein inhibits interferon-induced nuclear import of STATs. *Journal of medical virology* 73: 536-547, 2004.

94. **Morral N, Edenberg HJ, Witting SR, Altomonte J, Chu T, and Brown M.** Effects of glucose metabolism on the regulation of genes of fatty acid synthesis and triglyceride secretion in the liver. *Journal of lipid research* 48: 1499-1510, 2007.

95. **Moyers JS, Bilan PJ, Zhu J, and Kahn CR.** Rad and Rad-related GTPases interact with calmodulin and calmodulin-dependent protein kinase II. *J Biol Chem* 272: 11832-11839, 1997.

96. **Nerup J, Platz P, Andersen OO, Christy M, Lyngsoe J, Poulsen JE, Ryder LP, Nielsen LS, Thomsen M, and Svejgaard A.** HL-A antigens and diabetes mellitus. *Lancet* 2: 864-866, 1974.

97. **Newberry EP, Xie Y, Kennedy SM, Luo J, and Davidson NO.** Protection against Western diet-induced obesity and hepatic steatosis in liver fatty acid-binding protein knockout mice. *Hepatology (Baltimore, Md* 44: 1191-1205, 2006.

98. **Osman MA and Cerione RA.** Iqg1p, a yeast homologue of the mammalian IQGAPs, mediates cdc42p effects on the actin cytoskeleton. *The Journal of cell biology* 142: 443-455, 1998.

99. **Owerbach D and Gabbay KH.** Localization of a type I diabetes susceptibility locus to the variable tandem repeat region flanking the insulin gene. *Diabetes* 42: 1708-1714, 1993.

100. **Paez J and Sellers WR.** PI3K/PTEN/AKT pathway. A critical mediator of oncogenic signaling. *Cancer treatment and research* 115: 145-167, 2003.

101. **Park KJ, Choi SH, Choi DH, Park JM, Yie SW, Lee SY, and Hwang SB.** 1Hepatitis C virus NS5A protein modulates c-Jun N-terminal kinase through interaction with tumor necrosis factor receptor-associated factor 2. *J Biol Chem* 278: 30711-30718, 2003.

102. **Pasquinelli C, Garreau F, Bougueleret L, Cariani E, Grzeschik KH, Thiers V, Croissant O, Hadchouel M, Tiollais P, and Brechot C.** Rearrangement of a common cellular DNA domain on chromosome 4 in human primary liver tumors. *Journal of virology* 62: 629-632, 1988.

103. **Pece S, Chiariello M, Murga C, and Gutkind JS.** Activation of the protein kinase Akt/PKB by the formation of E-cadherin-mediated cell-cell junctions. Evidence for the association of phosphatidylinositol 3-kinase with the E-cadherin adhesion complex. *J Biol Chem* 274: 19347-19351, 1999.

104. **Philp AJ, Campbell IG, Leet C, Vincan E, Rockman SP, Whitehead RH, Thomas RJ, and Phillips WA.** The phosphatidylinositol 3'-kinase p85alpha gene is an oncogene in human ovarian and colon tumors. *Cancer research* 61: 7426-7429, 2001.

105. **Pinkse GG, Voorhoeve MP, Noteborn M, Terpstra OT, Bruijn JA, and De Heer E.** Hepatocyte survival depends on beta1-integrin-mediated attachment of hepatocytes to hepatic extracellular matrix. *Liver Int* 24: 218-226, 2004.

106. **Postic C, Dentin R, Denechaud PD, and Girard J.** ChREBP, a Transcriptional Regulator of Glucose and Lipid Metabolism. *Annu Rev Nutr* 27: 179-192, 2007.

107. **Qin LX and Tang ZY.** The prognostic molecular markers in hepatocellular carcinoma. *World J Gastroenterol* 8: 385-392, 2002.

108. **Raclot T.** Selective mobilization of fatty acids from adipose tissue triacylglycerols. *Progress in lipid research* 42: 257-288, 2003.

109. **Ren JG, Li Z, Crimmins DL, and Sacks DB.** Self-association of IQGAP1: characterization and functional sequelae. *J Biol Chem* 280: 34548-34557, 2005.

110. **Rogler CE, Sherman M, Su CY, Shafritz DA, Summers J, Shows TB, Henderson A, and Kew M.** Deletion in chromosome 11p associated with a hepatitis B integration site in hepatocellular carcinoma. *Science (New York, NY* 230: 319-322, 1985.

111. **Scemons D.** Are you up-to-date on diabetes medications? *Nursing* 37: 45-49; quiz 49-50, 2007.

112. **Schmidt VA, Chiariello C.S., Capilla E., Pessin J.E., Miller F., Bahou W.F.** Development of hepatocellular carcinoma in Iqgap2-deficient mice is mediated by dominant negative inhibition of IQGAP1, Submitted.

113. **Schmidt VA, Scudder L, Devoe CE, Bernards A, Cupit LD, and Bahou WF.** IQGAP2 functions as a GTP-dependent effector protein in thrombin-induced platelet cytoskeletal reorganization. *Blood* 101: 3021-3028, 2003.

114. **Shaat N and Groop L.** Genetics of gestational diabetes mellitus. *Current medicinal chemistry* 14: 569-583, 2007.

115. **Shayesteh L, Lu Y, Kuo WL, Baldocchi R, Godfrey T, Collins C, Pinkel D, Powell B, Mills GB, and Gray JW.** PIK3CA is implicated as an oncogene in ovarian cancer. *Nature genetics* 21: 99-102, 1999.

116. **Shimano H.** SREBP-1c and TFE3, energy transcription factors that regulate hepatic insulin signaling. *Journal of molecular medicine (Berlin, Germany)* 85: 437-444, 2007.

117. **Steinberg SJ, Kemp S, Braiterman LT, and Watkins PA.** Role of very-long-chain acyl-coenzyme A synthetase in X-linked adrenoleukodystrophy. *Annals of neurology* 46: 409-412, 1999.

118. **Storlien L, Oakes ND, and Kelley DE.** Metabolic flexibility. *The Proceedings of the Nutrition Society* 63: 363-368, 2004.

119. **Swart-Mataraza JM, Li Z, and Sacks DB.** IQGAP1 is a component of Cdc42 signaling to the cytoskeleton. *J Biol Chem* 277: 24753-24763, 2002.

120. **Taghibiglou C, Rashid-Kolvear F, Van Iderstine SC, Le-Tien H, Fantus IG, Lewis GF, and Adeli K.** Hepatic very low density lipoprotein-ApoB overproduction is associated with attenuated hepatic insulin signaling and overexpression of protein-tyrosine phosphatase 1B in a fructose-fed hamster model of insulin resistance. *J Biol Chem* 277: 793-803, 2002.

121. **Taules M, Rodriguez-Vilarrupla A, Rius E, Estanyol JM, Casanovas O, Sacks DB, Perez-Paya E, Bachs O, and Agell N.** Calmodulin binds to p21(Cip1) and is involved in the regulation of its nuclear localization. *J Biol Chem* 274: 24445-24448, 1999.

122. **Taylor JR and Campbell KM.** Home monitoring of glucose and blood pressure. *American family physician* 76: 255-260, 2007.

123. **Tedeschi H.** Old and new data, new issues: the mitochondrial DeltaPsi. *Biochimica et biophysica acta* 1709: 195-202, 2005.

124. **Venturelli CR, Kuznetsov S, Salgado LM, and Bosch TC.** An IQGAP-related gene is activated during tentacle formation in the simple metazoan Hydra. *Development genes and evolution* 210: 458-463, 2000.

125. **Wang GS, Olsson JM, Eriksson LC, and Stal P.** Diet restriction increases ubiquinone contents and inhibits progression of hepatocellular carcinoma in the rat. *Scandinavian journal of gastroenterology* 35: 83-89, 2000.

126. **Wang JS and Groopman JD.** DNA damage by mycotoxins. *Mutation research* 424: 167-181, 1999.

127. **Wang S, Watanabe T, Noritake J, Fukata M, Yoshimura T, Itoh N, Harada T, Nakagawa M, Matsuura Y, Arimura N, and Kaibuchi K.** IQGAP3, a novel effector of Rac1 and Cdc42, regulates neurite outgrowth. *Journal of cell science* 120: 567-577, 2007.

128. **Wang X, Wang R, Nemcek TA, Cao N, Pan JY, and Frevert EU.** A self-contained 48-well fatty acid oxidation assay. *Assay Drug Dev Technol* 2: 63-69, 2004.

129. **Wei E, Gao W, and Lehner R.** Attenuation of adipocyte triacylglycerol hydrolase activity decreases basal fatty acid efflux. *J Biol Chem* 282: 8027-8035, 2007.

130. **Weissbach L, Settleman J, Kalady MF, Snijders AJ, Murthy AE, Yan YX, and Bernards A.** Identification of a human rasGAP-related protein containing calmodulin-binding motifs. *J Biol Chem* 269: 20517-20521, 1994.

131. **WHO.** Diabetes: World Health Organization, 2006.

132. **Winter WE, Nakamura M, and House DV.** Monogenic diabetes mellitus in youth. The MODY syndromes. *Endocrinology and metabolism clinics of North America* 28: 765-785, 1999.

133. **Xu J, Chang V, Joseph SB, Trujillo C, Bassilian S, Saad MF, Lee WN, and Kurland IJ.** Peroxisomal proliferator-activated receptor alpha deficiency diminishes insulin-responsiveness of gluconeogenic/glycolytic/pentose gene expression and substrate cycle flux. *Endocrinology* 145: 1087-1095, 2004.

134. **Xu J, Gowen, L., Raphalides, C., Hoyer, K.K., Weinger, J.G., Renard, M., Troke, J.J., Vaitheesyaran, B., Paul Lee, W.N., Saad, M.F., Sleeman, M.W., Teitell, M.A., Kurland, I.J.** Decreased Hepatic Futile Cycling Compensates for Increased Glucose Disposal in the Pten Heterodeficient Mouse. *Diabetes* 55: 3372-3380, 2006.

135. **Yen TC, Chen YS, King KL, Yeh SH, and Wei YH.** Liver mitochondrial respiratory functions decline with age. *Biochemical and biophysical research communications* 165: 944-1003, 1989.

136. **Zhang H, Ozaki I, Mizuta T, Matsuhashi S, Yoshimura T, Hisatomi A, Tadano J, Sakai T, and Yamamoto K.** Beta 1-integrin protects hepatoma cells from chemotherapy induced apoptosis via a mitogen-activated protein kinase dependent pathway. *Cancer* 95: 896-906, 2002.

137. **Zhu Y, Zhong X, Zheng S, Ge Z, Du Q, and Zhang S.** Transformation of immortalized colorectal crypt cells by microcystin involving constitutive activation of Akt and MAPK cascade. *Carcinogenesis* 26: 1207-1214, 2005.